AD_____

Award Number: W81XWH-13-1-0050

TITLE: Development of Ultrasound to Measure In-vivo Dynamic Cervical Spine Intervertebral Disc Mechanics

PRINCIPAL INVESTIGATOR: Brian Snyder

CONTRACTING ORGANIZATION: Beth Israel Deaconess Medical Center
Boston, MA 02215

REPORT DATE: January 2015

TYPE OF REPORT: Annual Report

PREPARED FOR: U.S. Army Medical Research and Materiel Command
Fort Detrick, Maryland 21702-5012

REPORT DOCUMENTATION PAGE

Form Approved
OMB No. 0704-0188

1. REPORT DATE	**2. REPORT TYPE**	**3. DATES COVERED**
January 2015	**Annual**	**27 Dec 2013 - 26 Dec 2014**

4. TITLE AND SUBTITLE

Development of Ultrasound to Measure In-vivo Dynamic Cervical Spine Intervertebral Disc Mechanics

5a. CONTRACT NUMBER

5b. GRANT NUMBER
W81XWH-13-1-0050

5c. PROGRAM ELEMENT NUMBER

6. AUTHOR(S)

Brian Snyder

E-Mail: Brian.Snyder@childrens.harvard.edu

5d. PROJECT NUMBER

5e. TASK NUMBER

5f. WORK UNIT NUMBER

7. PERFORMING ORGANIZATION NAME(S) AND ADDRESS(ES)

Beth Israel Deaconess Medical Center
330 Brookline Avenue, Boston, MA

Medical College of Wisconsin
8701 W Watertown Plank Rd, Milwaukee, WI 53226

8. PERFORMING ORGANIZATION REPORT

9. SPONSORING / MONITORING AGENCY NAME(S) AND ADDRESS(ES)

U.S. Army Medical Research and Materiel Command
Fort Detrick, Maryland 21702-5012

10. SPONSOR/MONITOR'S ACRONYM(S)

11. SPONSOR/MONITOR'S REPORT NUMBER(S)

12. DISTRIBUTION / AVAILABILITY STATEMENT

Approved for Public Release; Distribution Unlimited

13. SUPPLEMENTARY NOTES

14. ABSTRACT

Neck pain is pervasive problems in military population, especially in those working in vibrating environments. Previous studies show neck pain is strongly associated with degeneration of Intervertebral Disc (IVD), which is commonly caused by repetitive loading and aging. To reduce the risk of cervical spine disease, there is a need to measure the effect by helmet, equipment and seating. However, in-vivo displacement and loading condition of cervical spine are difficult to measure during operation. Clinical ultrasound (US) is being explored as a valuable tool to image motion of the cervical spine, specifically vertebral motion and intervertebral disc deformation. A dual US imaging system is being developed to measure 3D motion of contiguous cervical vertebrae and IVD strain (Δheight of IVD/original IVD height) of intervening functional spine units (FSU). This system was validated ex-vivo using cadaveric C-spines mounted in a servo-hydraulic material testing machine by comparing dynamic US measurement to direct measurements using a linear variable differential transformer (LVDT) system in our previous 2013-2014 annual progress report. In year 2014-2015, we further developed the performance of hardware/software of dual ultrasound system. The capability of dual US to measure C-spine properties in-vivo in simulation environment is currently being tested. Biomechanics finite element(FE) models were developed to examine how dynamic forces applied to the occipital-atlantal junction (i.e. C1) are transferred to the subaxial C-spine.

15. SUBJECT TERMS

16. SECURITY CLASSIFICATION OF:			**17. LIMITATION OF ABSTRACT**	**18. NUMBER OF PAGES**	**19a. NAME OF RESPONSIBLE PERSON**
					USAMRMC
a. REPORT	**b. ABSTRACT**	**c. THIS PAGE**			**19b. TELEPHONE NUMBER** *(include area code)*
U	U	U	UU	50	

Table of Contents

1. ABSTRACT

Neck pain is pervasive problems in military population, especially in those working in vibrating environments. Previous studies show neck pain is strongly associated with degeneration of Intervertebral Disc (IVD), which is commonly caused by repetitive loading and aging. To reduce the risk of cervical spine disease, there is a need to measure the effect by helmet, equipment and seating. However, *in-vivo* displacement and loading condition of cervical spine are difficult to measure during operation. Clinical ultrasound (US) is being explored as a tool to image motion of the cervical spine, specifically vertebral kinematics and intervertebral disc deformation. A dual US imaging system is being developed to measure 3D motion of contiguous cervical vertebrae and IVD strain (Δheight of IVD/original IVD height) of intervening functional spine units (FSU). This system was validated *ex-vivo* using cadaveric C-spines mounted in a servo-hydraulic material testing machine by comparing dynamic US measurement to direct measurements using the linear variable differential transformer (LVDT) of the hydraulic test system. Over the past year of support, 2014-2015, we improved the performance of hardware and software for the dual ultrasound system. The capability of the dual US to measure C-spine elastic and viscoelastic properties *in-vivo* under conditions simulating vibrations over a range of frequencies and amplitudes is currently being tested. Finite element (FE) models of the human cervical spine have been developed to examine the dynamic response of the cervical spine functional spine units in response to forces and moments applied to the head and neck..

2. INTRODUCTION

In the year 2013, we developed a unique dual US system that can non-invasively measure IVD deformation and mechanical compliance *ex-vivo*, and provide real-time images of IVDs and dynamic vertebral motion *in-vivo* during simulated tasks. A transfer function that modeled the non-linear displacement of human cadaveric cervical spine functional spine units was developed to account for the differential elasticity during compression or tension.

The project focus of 2014 was to apply the dual US *in-vivo* and model analytically the elastic and viscoelastic behavior of the cervical spine in response to cyclic loading. Compared to using the US system to image the C-spine *ex-vivo*, using the dual US system to image the C-spine *in-vivo* was much more challenging, affected by inadvertent human motion and inconsistent muscle activity that served to dampen the system. 2014 accomplishments:

1. Improved software for dual US system by developing a mathematical algorithm that corrects signal drift during tracking of vertebrae during long duration ultrasound imaging. This significantly increased tracking accuracy for *in-vivo* US imaging;
2. Developed system to apply *in-vivo* static and dynamic cyclic loads to the cervical spine at known forces, displacements and frequencies allowing derivation of the transfer function for C-spine FSU's C4-5;
3. Established a robust protocol for *ex-vivo* FSU/IVD fatigue testing. Elastic, viscoelastic and failure properties of FSU determined for C-spine FSUs that were incorporated into material properties of C-spine FEM used to simulate cyclic loading and fatigue behavior of C-spine. The biomechanics properties (compliance or damping coefficient) of the IVD have been correlated to clinical measures of FSU health and function measured by MRI (Pfirrmann grade)

3. PROGRESS

3.1 Ultrasound System Development and Validation (Continuation of Task 1 and 2 in Aim 1)

A blockmatching algorithm was used to compare two consecutive US images and map the lateral (i.e. perpendicular to U/S beam) and axial (parallel to U/S beam) displacement of pixels forming the image profiles of the vertebrae. This algorithm was previously validated using *ex-vivo* cadaver cervical spines. However during real time *in-vivo* tracking of cervical vertebrae, new challenges emerged that did not occur in the cadaver test: it was difficult to maintain the dual ultrasound probes in the standardized fixed position in direct acoustic contiguity with the vertebrae during dynamic flexion/extension motion. The previous methods failed to correct signal drift, which was accumulated during long duration US tracking. Accuracy of FSU kinematics especially during high frequency motion was limited.

Based on the work of Rahimi et al. 2001, we developed a mathematical model suitable to correct signal drift during tracking of vertebrae during long duration ultrasound imaging. This method relaxes the restriction that only temporally adjacent ultrasound frames are compared (known as frame-to-frame tracking) to calculate the relative interval motion of the vertebra. It allows high-quality, non-sequential measurements to be used in-lieu of poor quality, sequential measurements. When estimating the position of vertebrae, the motion tracking method takes into account the change in position between the current frame and the previous frame, as well as other previous spatially related image frames tracking the position of the vertebra. This expanded set of high quality US images is now used to analyze the ultrasound radio frequency (RF) data.

The accuracy and precision of US measurements of vertebral motion were validated using a PMMA phantom to track rigid body motion over a range of frequencies. A PMMA block was secured to the actuator piston of a servohydraulic materials testing machine to which 1mm sinusoidal displacements were applied over a range of frequencies for 20 seconds (1000 frames).

The block was fully immersed in a water bath to allow acoustic coupling to the US probe. The applied displacement was compared between direct measurements from the linear voltage differential transformer (LVDT) in line with the actuator and that derived using a single US device and the motion tracking software (Figure 1).

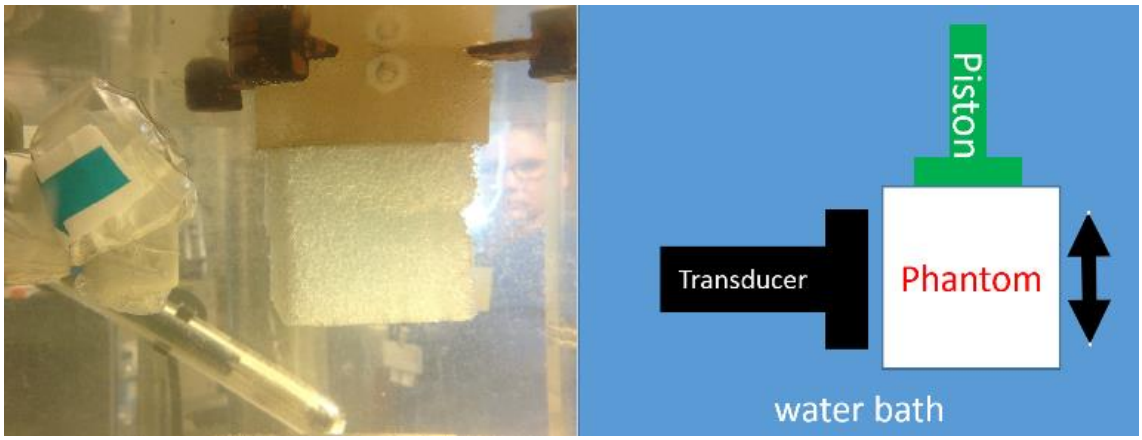

Figure 1: Ultrasound imaging of PMMA phantom secured to actuator piston of materials testing machine. Measurements were compared between derived displacements using tracking algorithm and LVDT.

Six different Regions of Interest (ROIs) on the phantom were chosen to evaluate the precision of the tracking algorithm. For applied frequencies 1 - 8 Hz, the mean absolute error (MAE) between translational motion measured using the US tracking system and the LVDT ranged from 0.0227 to 0.0508 mm (Figure 2). The overall average MAE of US measurements were 0.041 mm. No drift was observed during the course of scan (1000 frames). Accuracy was not significantly affected by motion frequency. Assuming typical IVD deformation of 0.8mm under 150N load, this corresponds to a 6.3% precision error in the US measured strain.

Software using the new tracking algorithm has been integrated into dual US package. The software has graphic user interface (Figure 3), which allows the operator to analyze the relative displacements of cervical vertebrae and the deformation of intervertebral discs (IVD). The program is written on C++ under open source framework and the executive files are compatible with different systems (tested in PC and Mac), which makes the dual ultrasound system (US) usable as a stand-alone system to acquire cervical spine motion data to calculate kinematics and IVD deformation.

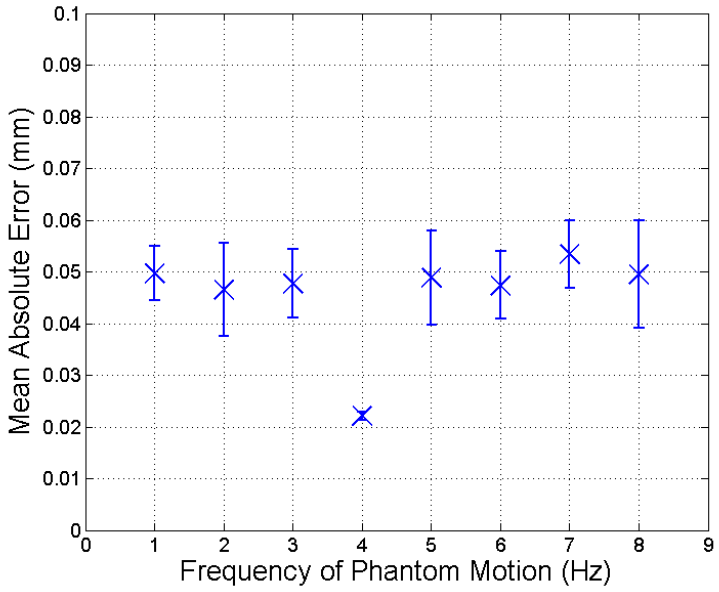

Figure 2: *The Mean Absolute Error for US vs. LVDT measurements of phantom motion plotted as function of applied frequency.*

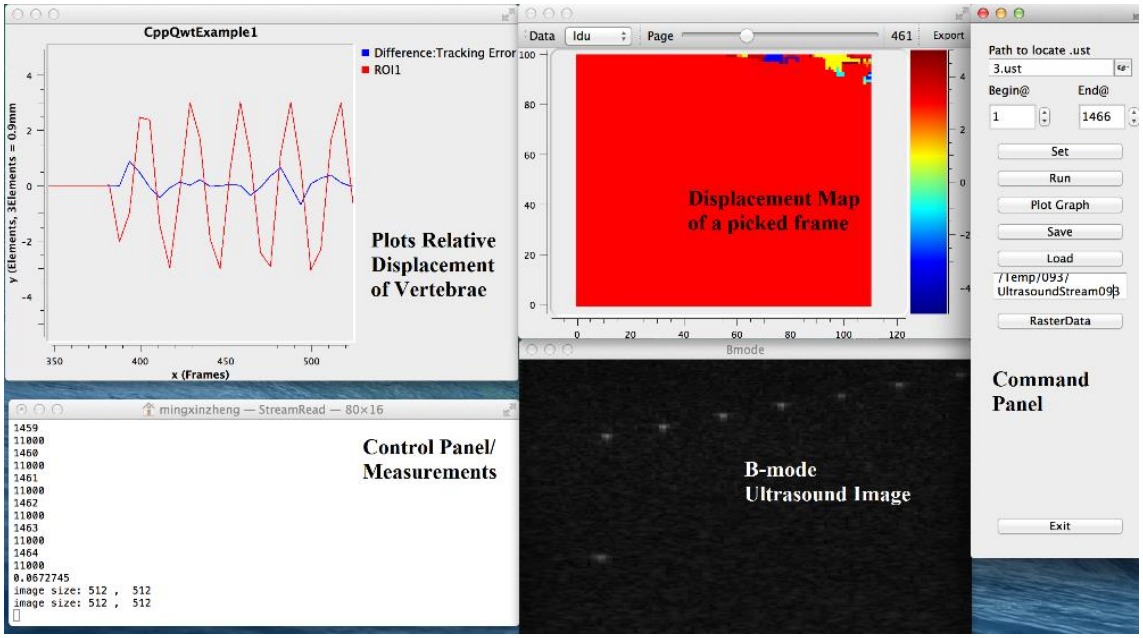

Figure 3: Graphic User Interface(GUI) of tracking software which allows users to analyze displacement of objects. Upper left plot is the displacement curve. Upper middle window plots the displacement map between frame pairs. Since we are applying this program to track a rigid phantom, all points inside phantom show the same displacement. B-mode image of phantom is shown lower middle, with measurements/image details shown in lower right.

3.2 *Ex-vivo* Hydration vs IVD Compliance and Cervical Spine Health and Integrity (Task 4 and 6)

Methodology to measure the mechanical properties of single and contiguous FSUs using intact cadaver specimens C2-C7 was developed. Previous *ex-vivo* experiments were conducted on isolated cervical spine FSU's which fail to replicate physiological conditions, especially the lordotic curvature of C-spine.

Contiguous segments C2-C7 from an 84-year-old male were used to develop the protocol. The posterior skin was retained to provide acoustic coupling for the dual US probes. The trachea and anterior skin were removed, but paracervical muscles and ligament were retained to maintain the tensile and compressive properties of the connective soft tissue envelope. The C2 and C7 vertebral bodies were potted in liquid plastic. Using minimally invasive technique, uniaxial, 5 mm diam. titanium pedicle screws were placed into the vertebral bodies, just anterior to the transverse process, under fluoroscopic guidance. To maintain the cervical lordosis, a slightly bent, 5 mm diameter stainless steel interconnecting rod was secured in the tulip head connectors of contiguous pairs of pedicles screws, rigidly secured with set screws. Our method was slightly modified from pedicle screw placement protocol. The pedicle screws were placed in the vertebral bodies in an Anterior-Posterior (A-P) position to better control (limit) flexion/extension motion of "instrumented" FSU's during cyclic mechanical testing. By using variable lengths of interconnecting rods secured to different pedicle screw levels, different combinations of FSU's could be fixed or mobilized. The specimen was mounted in material testing system (Instron 8511, Norwood, MA) and loaded from 20 lbs. compression to 20 lbs. tension. Fluoroscopic images captured the position of the vertebral bodies during different loading conditions (Figure 4). Dual ultrasound transducers were positioned anteriorly and posteriorly to image the IVD and vertebral bodies anteriorly and spinous processes posteriorly. There was no movement between the fixed

FSUs during compression and tension (Figure 5), while the "empty" pedicle screws did not interfere with the motion of the mobile FSUs.

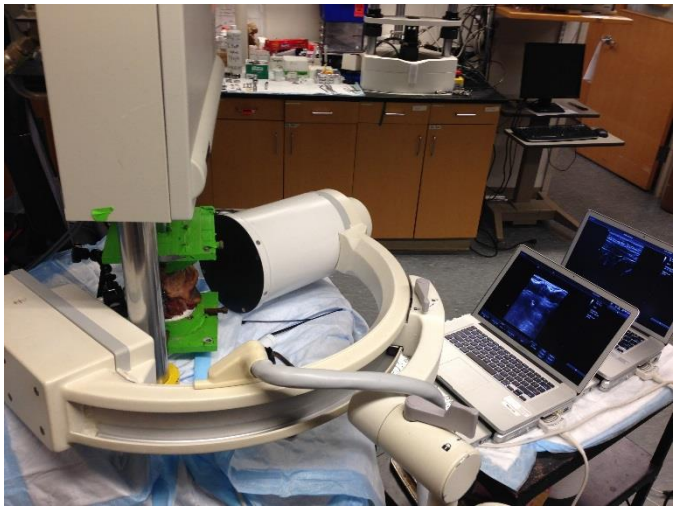

Figure 4: Cadaver testing with dual US and C-arm X-ray.

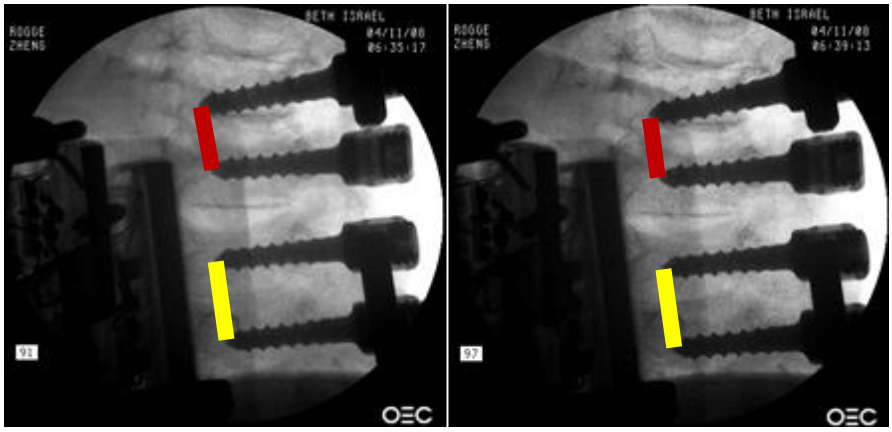

Figure 5: X-ray images of 20lbs. of tension (left) and 20lbs. compression (right). Black bars are US transducers. Relative motion occurred between mobile FSU levels (red bar length change = 0.1435mm), while no motion occurred between fixed FSU levels (yellow bar length change = 0.029mm, image resolution of X-ray is 0.3mm).

The stiffness and damping coefficients of the C4-C5 FSU (most common level of degenerative disease) were correlated with qualitative grading (Pfirrmann scale) of the IVD on MRI images (Figure 6). The ability of the dual US system to measure the biomechanical properties of the FSU was further validated by tracking the deformation of the C4-C5 FSU in real time during a standard creep test. Five fresh frozen, cadaveric human cervical spines, C2-T1, ages 54 - 67 years (Medcure, Portland, OR) were defrosted, the trachea, esophagus, and skin were removed. The surrounding para-cervical muscles and adipose tissue were retained. Each spine was subjected to

150N compressive creep test. Using minimally invasive technique, uniaxial, 5 mm diam. titanium pedicle screws were placed into the vertebral bodies under fluoroscopic guidance. Steel rods were used to fix C2-C4 FSUs and C5-T1 FSUs. The deformation of the C4-C5 IVD was measured by the dual US system and correlated with the real-time applied load.

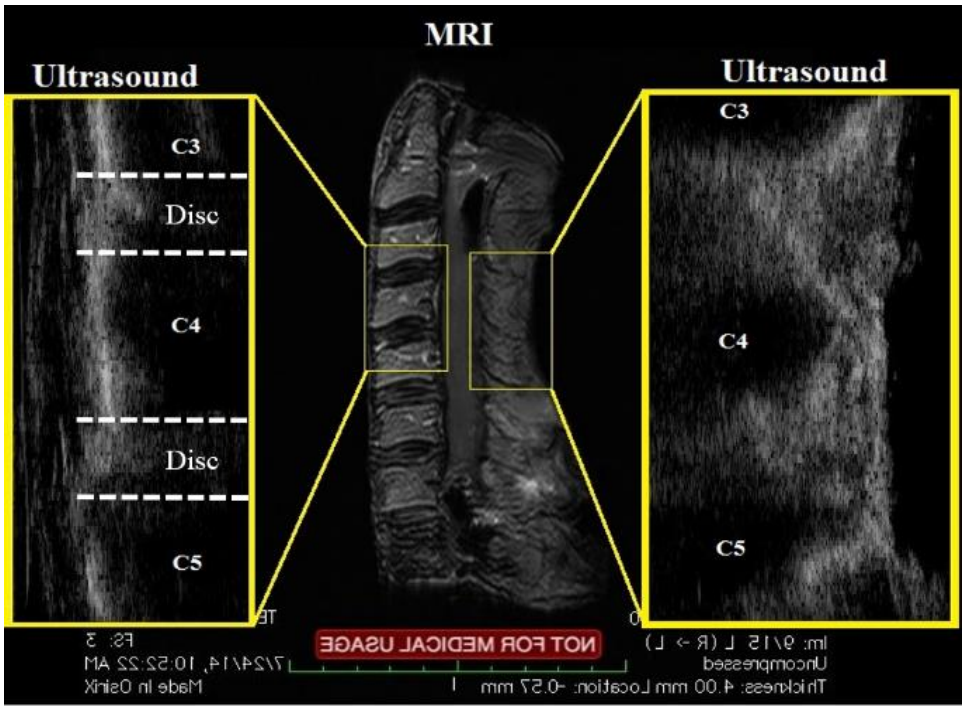

Figure 6: B-mode images of Ultrasound are compared to MRI sagittal image of cadaveric C-spine. Ultraound provides a magnified window of Functional Spinal Units in cadaver. One US acquired anterior vertebrae body and the other imaged posterior spinal processes.

Stiffness and damping coefficients of C4-C5 FSU were derived assuming a standard Voigt model comprised of an elastic spring and a viscous damper connected in parallel. Multivariate Linear Regression was used to calculate the stiffness of the elastic spring and the damping coefficient of viscous damper. These derived mechanical properties were compared to the structural integrity of the IVD measured on T_2 weighted MRI images of each FSU based on the Pfirrmann grading system, which is the clinical standard for evaluating the "health" of the IVD. Grade 1 is healthy hydrated disc that shows homogeneous brightness on T_2 MRI image while black, collapsed, dehydrated IVD on T2 MRI image is graded 5.

The age of the cadaveric C-spine specimens' ranged from 50-70 years, and the Pfirrmann grades ranged from 2 to 4. For compressive creep, the stiffness of the C4-5FSU correlated better

with the Pfirrmann Grade than the damping coefficient (Table 1). Younger specimens with better IVD hydration and structural integrity tended to be more compliant compared to older specimens with higher Pfirmann grades.

Table 1 Material properties of C4-C5 FSU measured by dual ultrasound system

Specimen#	1	2	3	4	5
Stiffness (N/mm)	117.3	203.3	258.3	264.2	312.5
Damp Coefficient (N•s/mm)	1420	1497	1045	1534	1110
Pfirrmann Grade of IVD	2	3	3	3	4
Age of Specimen (years)	54	58	63	58	67

3.3 *In-vivo* Ultrasound Test in Simulated Environment (Task 7)

In order to derive a transfer function for the mechanical behavior of the cervical spine *in-vivo* in a consistent and reproducible way, we are developing a system that applies cyclic distraction/compression loads to the neck at known amplitudes and frequencies representative of those mounted troops are exposed to during military operations. Two different test systems have been explored, one that actively applies cyclic distraction to the head/neck, similar to cervical traction used to treat cervical injuries clinically and another system that applies a cyclic compressive load to the head/neck via an actuator lifting the seat in which the subject is sitting, more representative of the scenario for mounted troops. The distraction based system consists of a motorcycle helmet worn by the subject with an attached weight (10lb.) that applies a static compressive load to the cervical spine. The weighted helmet is connected by a cable to a solenoid powered actuator that "unloads" the spine by applying a variable traction load (0 to 20 lbs) to the head and neck in a cyclic fashion over a range of frequencies (Figure 7, Figure 8). A load cell interposed between the weight and the helmet measures the resultant force applied to the neck in real time (iLoad Mini, Loadstarsensor, Fremont, CA).

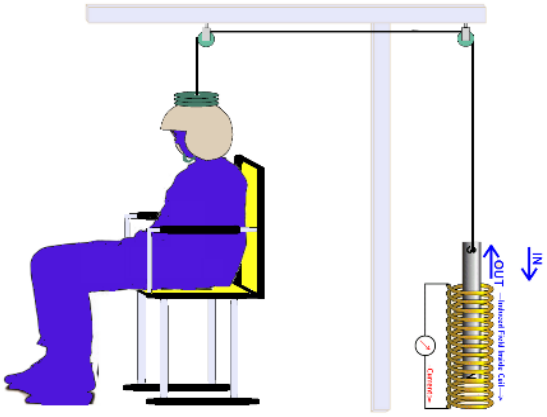

Figure 7: Schematic of cyclic load application system to head/neck of subject while sitting or standing in load frame.

Figure 8 Solenoid powered traction system for applying cyclic loads in-vivo

To ensure that the loading axis of the head and neck were collinear with the applied uniaxial force, a 5 point latch & link restraint system was used to fix the torso of the sitting subject to the load frame along the line of action of the cable. We tested the solenoid based traction system on ourselves by performing static and dynamic analysis of the compliance of C4-C5.

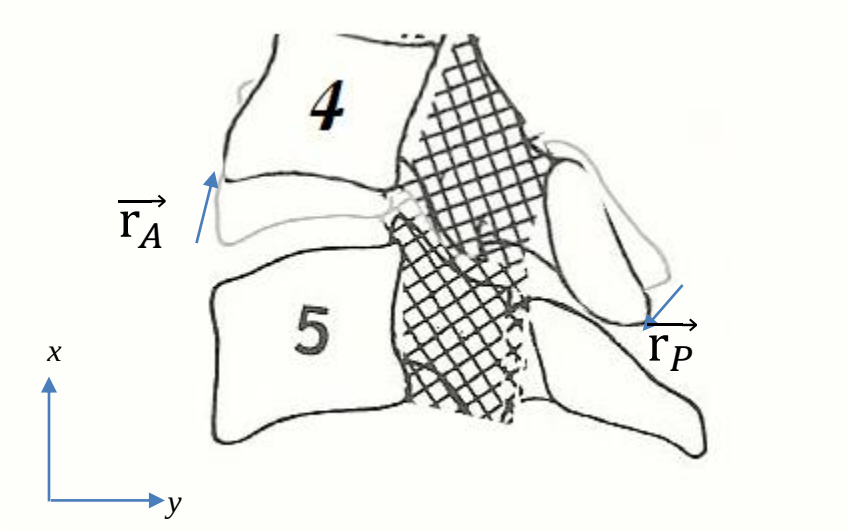

Figure 9: Simplified rigid body representation of cervical spine and coordinate system. The anterior profile of the vertebral body and IVD is imaged by the anteriorly positioned US probe, while the facet joint (cross-hatched region) and spinous process is imaged by the posteriorly positioned US probe (~60° relative to the anteriorly positioned probe)

The geometry of the vertebrae is assumed to remain constant during the course of the test. The surface contours of the cervical vertebrae imaged by the dual ultrasound probes can be depicted as a simplified 2D rigid-body (Figure 9). A global Cartesian coordinate system is fixed relative to the torso. The anterior and posterior motion of the C4-C5 FSU is represented by two vectors $\overrightarrow{r_A}$ (vertebral body endplate motion) and $\overrightarrow{r_P}$ (posterior element motion).The deformation of the C4-C5 IVD is estimated from the average displacement of these two vectors, while the flexion/extension angle of C4-C5 is estimated by calculating their vector cross-product:

$$Displacment = \frac{|\overrightarrow{r_A}|+|\overrightarrow{r_P}|}{2}$$

$$Angle = arctan\frac{r_{Ay}+r_{y0}}{r_{Ax}+r_{x0}} + arctan\frac{r_{Py}+r_{y0}}{r_{Px}+r_{x0}}$$

$r_{Ax}, r_{Ay}, r_{Px}, r_{Py}$ are the components of $\overrightarrow{r_A}$, $\overrightarrow{r_B}$ in the superior-inferior (X) and anterior-posterior (Y) directions, respectively in the loaded configuration and r_{x0} *and* r_{y0} are the components of these vectors in the unloaded configuration.

Static Testing: A static force from -10 lbs. (compression) to +15 lbs. (traction) was applied incrementally to the cervical spine using our controlled traction system (Figure 10). The dual US

system measured the resultant C4-C5 FSU's displacement and angular motion (Figure 10). The static compliance was derived from the slope of the displacement vs. load curve deduced by linear regression (Figure 11).

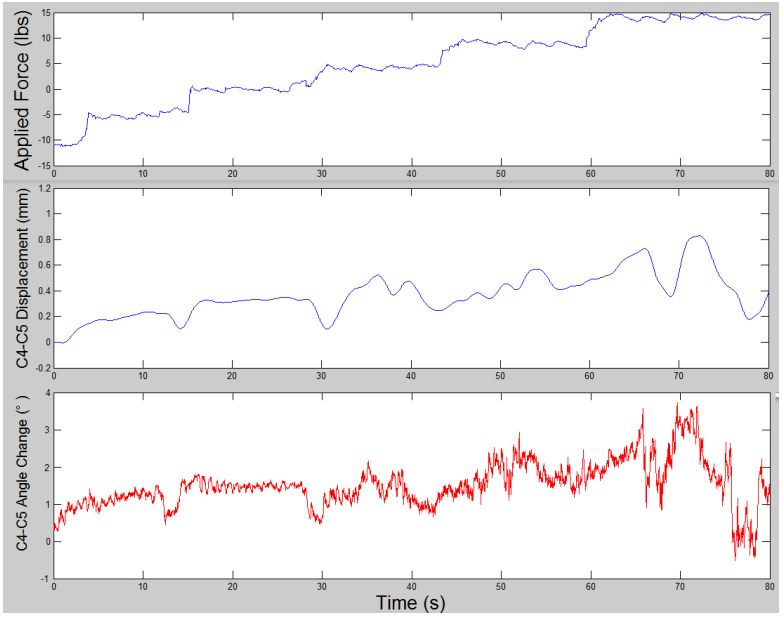

Figure 10: Sequential step loads applied to the head and neck witht resultant C4-C5 displacement and flexion/extension angle measured by US. The morphology of load-time curve and displacement-time curve demonstrated that the IVD displacement at C4-C5 correlated with the applied axial force. The resultant angular deformation implies that the applied axial force also exerts a moment on the cervical spine, a consequence of either the natural cervical spine lordosis, misalignment between the line of action of the applied load and the neutral axis of the cervical spine or voluntary muscle contraction by the subject.

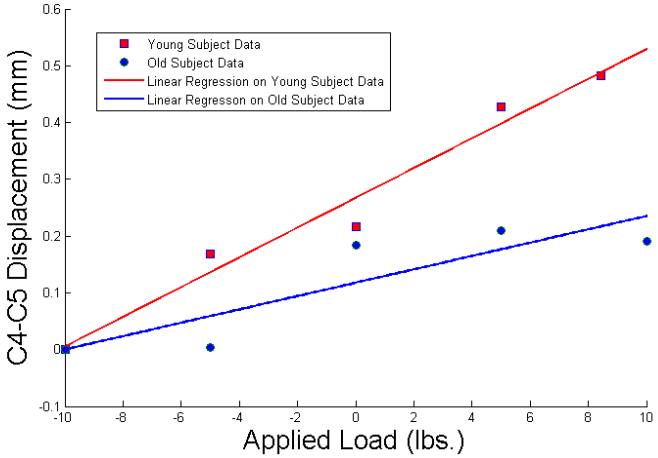

Figure 11: Elastic compliance of C4-C5 FSU using solenoid based traction device to apply static incremental loads R2= 0.97(red, 25y/o subject), 0.76 (blue, 56y/o subject). FSU tended to be more compliant for the younger human subject (0.00589mm/N) compared to older subject (0.00265mm/N).

Dynamic Testing: The feasibility of using US to measure the dynamic mechanical properties of cervical spine FSUs was explored by cyclically loading the neck between 0 to +20 lbs. The applied

load was a square-wave function (Figure 12a), the resultant displacement was highly non-linear (Figure 12b) exhibiting two distinct phases during loading and unloading: 1) there was little FSU displacement during the application and release of the traction load impulse; 2) there was creep deformation during the phase that the applied load was held constant. Analysis in the frequency domain facilitated derivation of the dynamic compliance, while the damping effect was calculated from the area under the displacement – load curve which physically represents the work lost in each cycle.

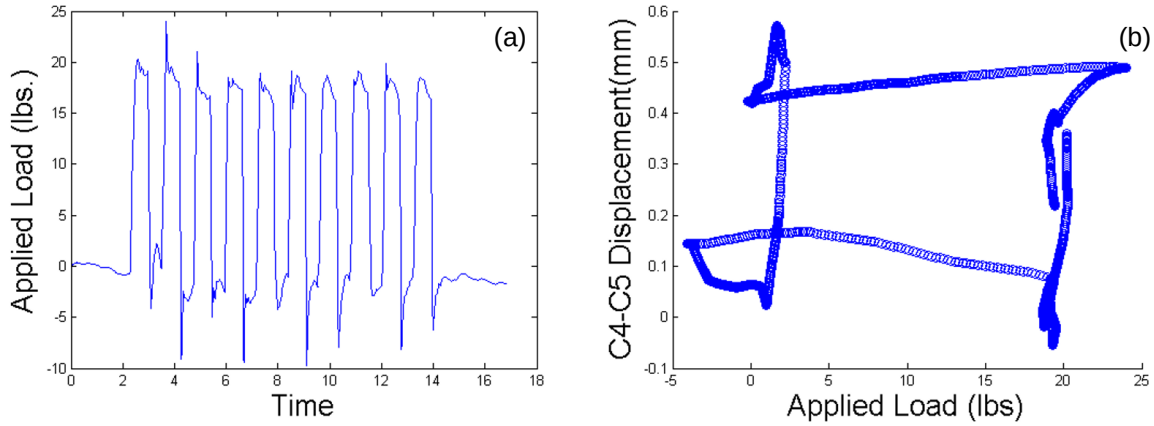

Figure 12: (a) Cyclic tensile step load applied by solenoid actuator; (b) resultant C4-C5 FSU deformation measured by dual US system.

Dynamic frequency analysis demonstrated the relative power spectra of applied loads and displacements (Figure 13). The highest peak in the frequency spectrum corresponded to the load and displacement at the applied frequency of the square wave and was used to filter out higher frequency "noise". Dynamic compliance was derived from the ratio of the C4-C5 FSU deformation in response to the applied load at the applied frequency. The 25 y/o subject had a more compliant C4-C5 FSU than the 56 y/o subject at all frequencies, but the compliance decreased at higher frequencies. The compliance of the C4-C5 FSU for the 56 y/o subject changed little as a function of the applied frequency (Table 2). The damping coefficient was more affected by frequency than age (Table 3).

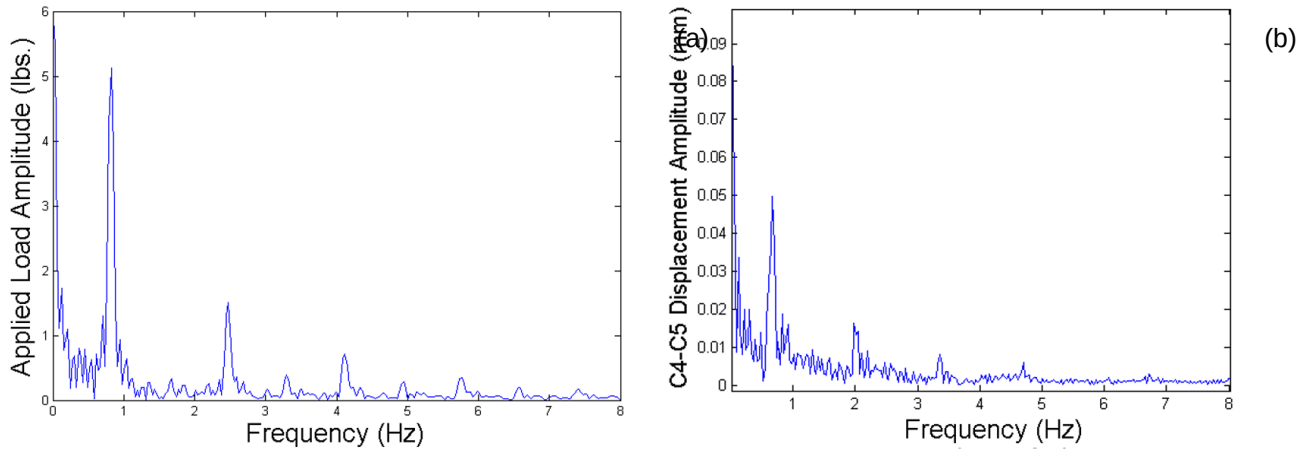

Figure 13:(a) Frequency analysis of applied load waveform (b) C4-C5 displacement measured by dual US in frequency domain

Table 2 Dynamic compliance as function of applied frequency and age

Frequency applied load	Dynamic Compliance mm/N		
	1 Hz	2Hz	3Hz
Younger Subject	0.0306	0.0242	0.0098
Older Subject	0.0111	0.0147	0.0123

Table 3 Work Loss as Function of Applied Frequency and Age

Frequency of load applied to neck	Area Estimate (Work loss) N × mm		
	1 Hz	2Hz	3Hz
Younger Subject	39.28	64.81	75.03
Older Subject	42.95	64.23	127.13

While this data is preliminary and limited to the PI and his graduate student, it demonstrates the promise of the proposed dynamic actuator to apply static and dynamic loads to the C-spine in a controlled, parametric fashion while simultaneously measuring the resulting deformation of C-spine FSU's using the dual US system thereby allowing calculation of the mechanical properties of the cervical spine *in-vivo* that dictate its functional performance. Differences in the transport of water through the poroelastic matrix of the IVD (which will be investigated further using diffusion based MRI) may account for the apparent affect of age and applied frequency on the compliance of the FSU. Additionally, reflexive contraction of the paracervical muscles to dampen forces applied to the cervical spine at higher loading frequencies could also account for the observed decrease in compliance and increase in energy dissipation at higher applied loading frequencies. EMG measurement of the activation of the paracervical muscles will elucidate this further.

These preliminary data identified a significant shortcoming of the solenoid actuator to apply cyclic distraction/compression loads at frequencies and amplitudes that will facilitate derivation of a universal transfer function for the mechanical behavior of the cervical spine FSUs *in-vivo* in a consistent and reproducible fashion or allow the application of different load profiles (sinusoidal, square wave, triangle, combinations thereof) that simulate the forces and moments applied to the head and neck of mounted troops during military maneuvers. Therefore we have developed a new system that uses a pneumatic powered load actuator that will allow more controlled cyclic load applications (Figure 14).

In this new design, the force is applied vertically through the seat that the subject is seated, transferred up the spine to the head and neck, which is secured in a helmet rigidly fixed to an adjustable cross-bar. At the point of attachment of the helmet to the cross-bar, there is a safety clutch that "breaks" for any applied load exceeding 25 lbs tension or compression (Figure 14B). Four co-axial linear bearing attached to the seat ensure precise up/down vertical movement without binding (Figure 14C). The maximum extension of the actuator is limited by a separate position sensing system. To safeguard against the risk of irregular air flow to the actuator, two redundant valves were added with an electronic PSI regulator. Additional safety features include an emergency "stop" switch that can be activated by either the subject or technician. Validation of the system and a full safety evaluation is being conducted using a Crash dummy (Humanetics, Plymouth, MI), an established test device in accordance with the USA Code of Federal Regulations. The dummy (Figure 15) has two 6-axis load cells on the top and bottom of its simulated C-spine, which provide real time load data applied to the neck. Preliminary studies on the break-away device were performed. The break-away device consists of 4 sets of commercially available wire break-away connecters (DCD Design, British Columbia, Canada), that break when the applied load exceeds the strength of internal wire. Repetitive loading studies that applied hyper-extension and hyper-compression to the dummy's spine demonstrated that the device released at -245.0±9.1 N (≈ 50 pounds) compressive load for a maximum

applied flexion moment of 9.1±3.4 Nm and 291±28 N (≈ 60 pounds) for a maximum applied extension moment of 14.1±8.5 Nm (Table 4). This exceeds our design criteria of 25-30lbs maximum load to be applied to the spine elements. Therefore customized wires from manufacturer will be used to attain this safety standard.

Figure 14: (A) front view of the updated design; (B) safety device release when applied force exceeds limit; (C) Lateral view of linear bearings and actuator placement

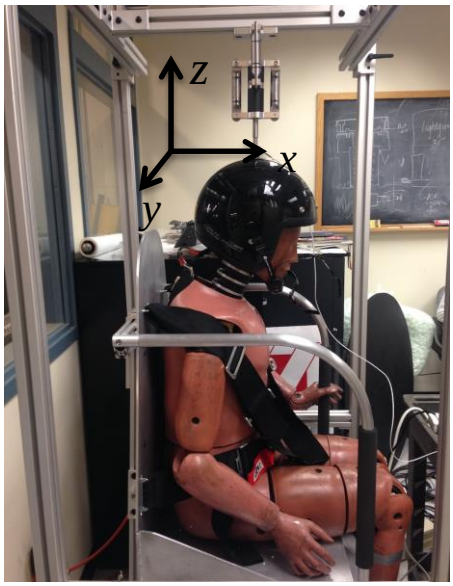

Figure 15: lateral view of the dummy in spine cyclic loading system and its Cartesian coordinates system

Table 4 Force and Moment Applied to Neck When Safety Device Breaks away

		Extension		Compression	
	Title	Average	STDEV	Avgrage	STDEV
Upper Neck (C1)	x-Axis Force(N)	66.6	8.7	-67.9	6.1
	y-Axis Force(N)	11.2	8.8	-7.5	1.3
	z-Axis Force(N)	272.3	28.8	-232.2	13.4
	x-Axis Moment(Nm)	1.0	0.8	-0.3	0.1
	y-Axis Moment(Nm)	-1.7	3.1	-3.3	1.1
	z-Axis Moment(Nm)	0.7	0.4	-0.7	0.2
Lower Neck (C7)	x-Axis Force(N)	61.2	9.4	-53.0	9.7
	y-Axis Force(N)	15.0	5.2	-6.6	1.0
	z-Axis Force(N)	290.9	27.9	-245.0	9.1
	x-Axis Moment(Nm)	1.8	1.1	-0.7	0.2
	y-Axis Moment(Nm)	14.1	8.5	-9.1	3.4
	z-Axis Moment(Nm)	1.0	1.0	-0.5	0.0

Cyclic loading of the dummy was attempted at different frequencies (1Hz-5Hz). At frequencies higher than 2Hz the pneumatic actuator was unable to apply a symmetric load-displacement curve; the rate of the applied load to lift the seat and dummy was slower than the rate of unloading. This is a result of the difference in the rate of pressurizing and depressurizing the pneumatic actuator. To compensate, we will use dead weights equivalent to the weight of the subject and the seat to "tare" the system, so that the pneumatic actuator only applies ± 25lbs. Cadaveric torsos with attached cervical spines C2-C7 will also be tested in this device prior to any *in-vivo* human tests to further establish the capabilities of the system to measure cervical spine FSU kinematics and IVD deformation. These data will be compared to similar tests conducted on isolated cervical spines using the Instron servohydraulic test system.

3.4 FE Model Validaition and Modification (Task 11) and Simulate Operation Loading Conditions (Task 12)

Finite element (FE) modeling for prediction of fatigue-related material property changes in cervical spine soft tissues is ongoing. N-code (HBM, Southfield, MI), was used to determine fatigue in the disc and it was able to reproduce fatigue in terms of number of cycles for a prescribed compressive load. However the formulation for calculation of Stress -Number of Cycles (SN) curve used is N-code is suitable for metals than for soft tissues as it is directly calculated from initial stiffness of the material, hence it is difficult to validate the results. Considering the observations, conclusions and challenges from the previous exercise a unique method of FE modeling was developed during the last quarter. The new method consists of coupling of Matlab (The Mathworks Inc., Natick, MA) and LS Dyna (Livermore Software Technology, Livermore, CA) to carry out fatigue simulations. This method was based, in part, on Qasim et al. 2012 and Qasim et al. 2014, who adopted a similar technique using Fortran in ADINA (ADINA R&D Inc., Watertown, Massachusetts).

Methodology: The computational algorithm which was used to model material property changes in cervical spine soft tissues related to repetitive axial compressive loading was outlined in Figure 16. Fatigue experiments with varying force amplitude and frequency were performed on bone-disc-bone segments at an interval of 10,000 cycles, up to 50,000 cycles. Quantified changes in intervertebral disc properties included: cycle-by-cycle compressive stiffness, intervertebral disc height, viscoelasticity, and tensile/compressive stiffness. The experimental results were used as input to the FE model as change in material properties due to fatigue.

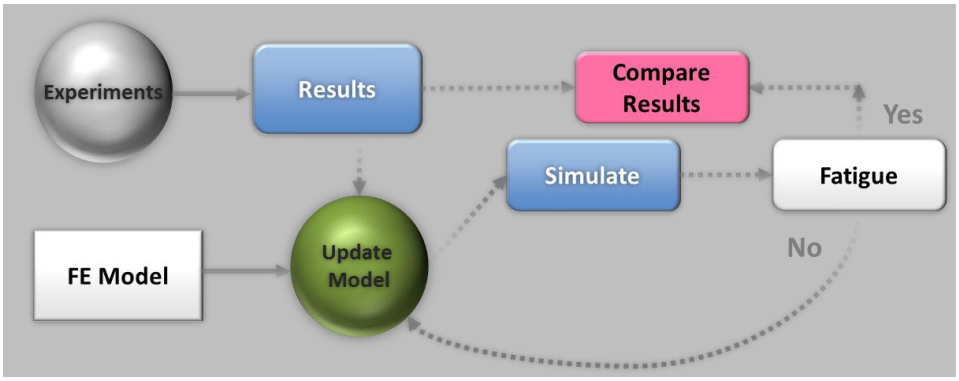

Figure 16: Schematic representation of vertebral disc segment under repetitive loading in a saline bath.

A FE model of a single cervical spine segment was developed. The IVD model consists of annulus fibrosus, nucleus pulposus, and superior and inferior endplates. The IVD model was discretized and programed with element-specific material properties with a script in Matlab. This process changing of material property values to model fatigue-related changes based on element-specific loading conditions after each cyclic loading procedure. The procedure consists of first performing a computational set of fatigue cycles in LS Dyna, then using a Matlab script to alter element-specific material properties of the soft tissues using Von Mises stress as the decision parameter, followed by the next fatigue cycle simulation in LS Dyna. Changes in IVD material properties are based on experimental results and will include scaling factors for the rate and magnitude of applied repetitive compressive loads. The degraded material properties will be incorporated for elements with Von Mises stress higher than the average. This report highlights experimental results from cervical spine segment testing to quantify fatigue-related material property changes and discretization of the finite element model, along with the experiments and FE fatigue modeling done before.

PART 1: Experiments

Experiments performed during the three quarters of last year are described below. Based on the experience of results from the previous set of experiments, the experimental protocol was updated. The experiments can be considered to be performed in three parts during the year and the protocol adopted during quarter 4, yielded best results and will be used for the future experiments.

Part 1: The experiments were performed to understand the effect of pure moment tests, viscoelastic tests in between fatigue tests and the inclusion of saline bath. Pure moment testing was first used to measure the bending response of cervical segments. Testing consisted of the static application of pure moments at 0.33Nm, 0.5Nm, 1Nm, 1.5Nm and 2Nm under flexion-extension and lateral bending (Wheeldon et al. 2006). Following pure moment testing, the segment was mounted on an anvil of MTS Systems, Eden Prairie, MN, which was immersed in a saline bath maintained at 34oC. The segment was allowed to acclimate in the water bath for 1 hour. Stress relaxation testing was then performed to quantify viscoelasticity of the segment. The specimen was compressed by 5% of the disc height and allowed to relax under the constant deformation. Stress relaxation testing was also performed prior to and following all fatigue sets. A Maxwell material model under fixed compressive strain was used to quantify viscoelasticity during the stress relaxation testing. Segments were then exposed to cyclic loading between 0 and -150N for 1000, 10,000 and 20,000 cycles at a frequency of 2Hz and pure moment and viscoelastic testing was performed between each fatigue set. The fatigue sets were performed at an interval of 24 hours.

Part 2: In this set of experiments five segments were tested under a cyclic compressive force of 0-150N at 2Hz up to 50000 cycles in two sets, in combination of 10,000-40,000 or 20,000-30,000 fatigue cycles. From the conclusion of experiments in previous quarter, it was observed that the pure moment tests affected the mechanical response of segments; therefore the pure moment tests were not performed prior to fatigue testing. Fatigue experiments were performed using the same MTS machine, the anvil of which was surrounded by a chamber saline bath, maintained at 35 ^{0}C. During testing, the segment was mounted on the anvil and allowed to acclimate in the water bath for 1 hour. A cyclic palpation of 10 cycles for 100N was performed to precondition the ligaments and tissues. Stress relaxation testing was then performed to assess viscoelasticity of the segment. The specimen was compressed by 100N force and was allowed to relax under the constant

deformation. A quasi-linear viscoelastic material model (Abramowitch 2004) was used to fit the stress relaxation data and the material parameters were obtained. After viscoelastic testing the spine segment was again allowed to rest in the saline bath for 30 mins. Segments were then exposed to cyclic loading between 0 and -150N for first set of fatigue cycles at a frequency of 2Hz, and the axial force and displacement were measured with respect to time. The details of segments tested are tabulated in Table 5. . After the first set of fatigue tests the segment was allowed to settle again for 30 minutes in the saline bath and then again viscoelastic test at the same strain (as done before fatigue test) was done. Further, after allowing the segment to settle for 30 minutes the pure moment test was performed on the segment. After the first set of fatigue loading the segment was again refrigerated and again the same protocol was followed when second set of fatigue tests were done.

Table 5: Details of segments tested under fatigue during Quarter 3.

S. N.	PMHS	Age (Yrs)	Sex	Mass (Kg)	FSU	Initial Height (mm)	Disc Area (mm^2)	Cycles Set 1	Cycle Set 2
1	HS-798	58	Male	57.61	C2-C3	7.824	274.961	10000	40000
2	HS-795	54	Male	107.05	C4-C5	9.809	355.028	10000	40000
3	HS-798	58	Male	57.61	C4-C5	8.457	407.961	20000	30000
4	HS-796	63	Male	56.7	C4-C5	5.404	211.459	30000	20000
5	HS-800	58	Female	79.83	C4-C5	6.485	447.486	10000	40000

Part 3: In this set of experiments the conclusion from the previous two sets of experiments was used pure moment test was completely removed from the protocol and all the fatigue sets were performed on bone disc bone segments, simultaneously with in 15 to 20 hours approximately. Four bone disc bone spine motion segments without posterior elements obtained from the cervical spines of human donors were fixed at cranial and caudal extents using polymethylmethacrylate (PMMA) (Table 6). Specimens were exposed to a protocol that included fatigue loading for 5 sets of 10,000 cycles with tension-compression and viscoelastic assessments prior to the first and after each 10,000-cycle fatigue set. Fatigue testing was performed with specimens submerged in a physiologic saline bath with temperature maintained at 34 deg C and consisted of repetitive

compression applied using the piston of an electrohydraulic testing device (MTS Systems, Eden Prairie, MN) between 0 and 150 N at 2 Hz using a sine wave function. Tension compression tests were performed at a quasi-static speed of 0.1 mm/s to 10% strain. The viscoelastic test involved compressing the specimen to 10% strain and allowing it to relax under the constant deformation. Disc height was measured from x-rays obtained after each fatigue set and was computed based on the average of three readings obtained at consistent locations in the disc. Axial force was measured at 100 Hz during the entire test using a uniaxial load cell attached to the piston. The segment was allowed to relax in the saline bath for 15 minutes after each 10,000-cycle fatigue set prior to the the initiation of the next test. The schematic representation of the experimental setup is provided in Figure 17.

Table 6: Details of segments tested under fatigue during Quarter 4..

S. N.	PMHS	Age (Yrs)	Sex	Mass (Kg)	FSU	Initial Height (mm)	Disc Area (mm^2)
1	HS 799	64	Female	48.1	C6-C7	8.13	318
2	HS-799	64	Female	48.1	C4-C5	6.05	283
3	HS-799	64	Female	48.1	C2-C3	7.47	195
4	HS-798	58	Male	57.61	C6-C7	7.78	442

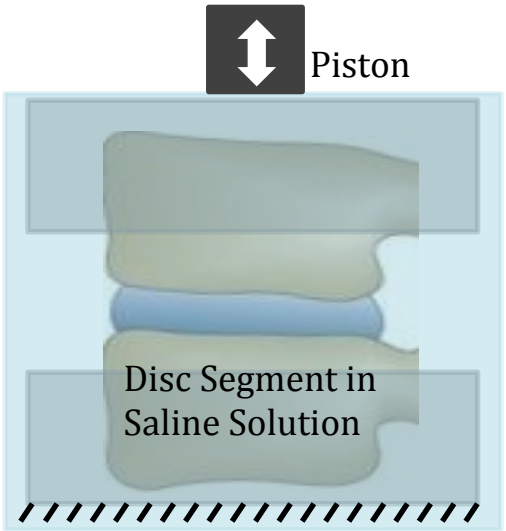

Figure 17: Schematic representation of vertebral disc segment under repetitive loading in a saline bath.

Quasi Linear Viscoelastic Model: A quasi-linear viscoelastic (QLV) material model (Abramowitch 2004) was used to fit the stress relaxation data and allow for the quantification of discrete material property constants to describe the viscoelastic behavior. The QLV theory models

the viscoelastic response of a material as a stress relaxation function formed using a series of discrete linear sections. The instantaneous stress resulting from a ramp strain is given as:

$$\sigma(t) = G(t) \times \sigma^e(\varepsilon) \tag{1}$$

where $\sigma(t)$ is the stress at any time t, $\sigma^e(\varepsilon)$ is the stress corresponding to an instantaneous strain, $G(t)$ is the reduced relaxation function representing the stress of the material divided by the stress after the initial ramp strain.

The complete stress history at any time t is then the convolution integral:

$$\sigma(t) = \int_{-\infty}^{t} G(t-\tau) \times \frac{\partial \sigma^e(t)}{\partial \varepsilon} \frac{\partial \varepsilon}{\partial \tau} \tag{2}$$

Where G is the reduced relaxation function, $\frac{\partial \sigma^e(t)}{\partial \varepsilon}$ represents the instantaneous elastic response, and $\frac{\partial \varepsilon}{\partial \tau}$ is the strain history. The reduced relaxation function proposed by (Toms et al. 2002) is:

$$G(t) = ae^{-bt} + ce^{-dt} + ge^{-ht} \tag{3}$$

Where, a, b, c, d, f, g are all constants. The instantaneous stress response is assumed to be represented through the nonlinear elastic relationship:

$$\sigma^e(\varepsilon) = A\left(e^{B\varepsilon} - 1\right) \tag{4}$$

Where, A and B are constants. Assuming that *t* starts at *0* instead of negative infinity, and substituting the strain history and the instantaneous stress response into the QLV model to obtain the stress history from t_0 (time at peak strain) to *t* (end of stress relaxation curve) we get:

$$\sigma(t > t_0) = \int_0^{t_0} \left\{ ae^{-b(t-\tau)} + ce^{-d(t-\tau)} + ge^{-h(t-\tau)} \right\} e^{B\gamma\tau} d\tau \tag{5}$$

Integrating and applying the limits we obtain:

$$\sigma(t > t_0) = AB\gamma\left[\frac{ae^{-bt}e^{(b+B\gamma)t_0}}{b+B\gamma} + \frac{ce^{-dt}e^{(d+B\gamma)t_0}}{d+B\gamma} + \frac{ge^{-bt}e^{(h+B\gamma)t_0}}{h+B\gamma}\right] - AB\left[\frac{ae^{-bt}}{b+B\gamma} + \frac{ce^{-dt}}{d+B\gamma} + \frac{ge^{-ht}}{h+B\gamma}\right] \quad (6)$$

This analytical form is used to optimize the QLV material parameters in MATLAB.

Results:

Part 1: Piston stroke (relative strain / piston displacement for respective cycle) and segmental stiffness was calculated from the force-displacement response measured for each cycle. For the first 1,000 cycles the piston stroke was well as stiffness was almost constant, which indicated that segmental axial stiffness for that specimen remained approximately unchanged during the 1,000 cycles. Stiffness gradually increased with repetitive compressive loading during the 10,000 cycles, more dramatically after the first 500 cycles. Following the 10,000 cycles, segmental stiffness again decreased during the initiation of the 20,000-cycle set as shown in Figure 18. To investigate the effects of the pure moment protocol and saline bath on fatigue, two segments were tested without saline solution, but included pure moment testing before and after fatigue sets. Increased segmental stiffness was evident during the tests, but occurred considerably earlier in these tests conducted without saline bath. Those specimens demonstrated considerable stiffness change during the first 1,000 cycles (~27%) (Figure 19) that was not evident in the prior tests that included saline. However, stiffness change between tests was considerably lower, presumably because of the large change during the first 1,000 cycles.

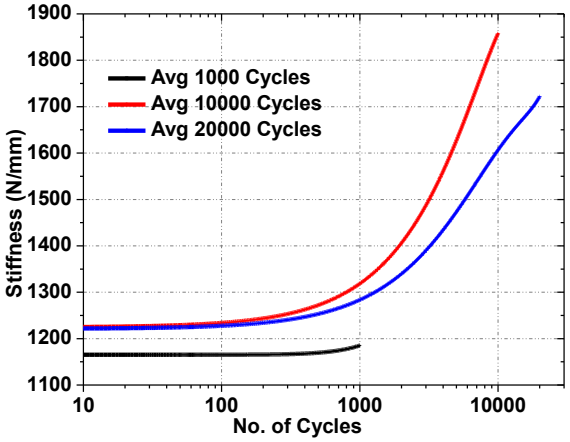

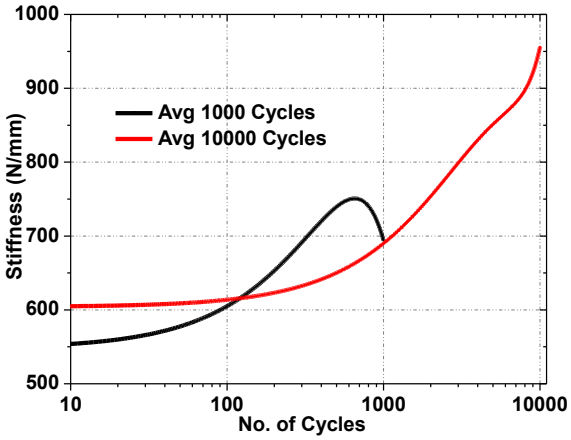

Figure 18: Average stiffness for 1st set of segments *Figure 19: Average stiffness for 2nd set of segments*

Two additional segments were tested without saline bath or pure moment testing. Similar to the tests above, a greater and earlier stiffness change was observed during the first 1,000 cycles (Figure 20). Likewise, 12 and 16% increase in stiffness was demonstrated between the end of the 1,000-cycle set and the beginning of the 10,000-cycle set. It was likely due to dehydration of the specimen that occurred when not in the saline bath, which leads to an accelerated decay in soft tissues that manifests biomechanically as increased stiffness.

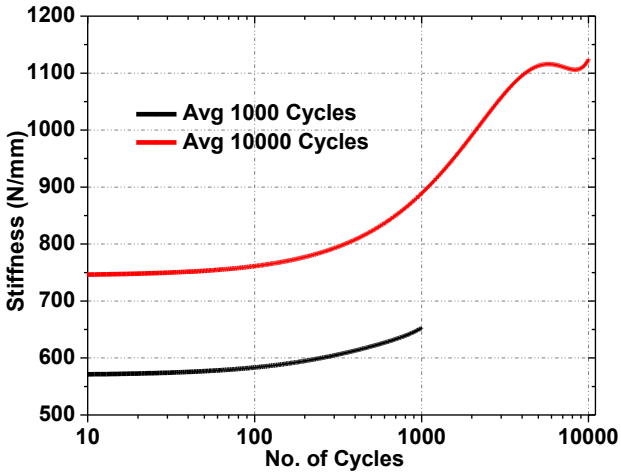

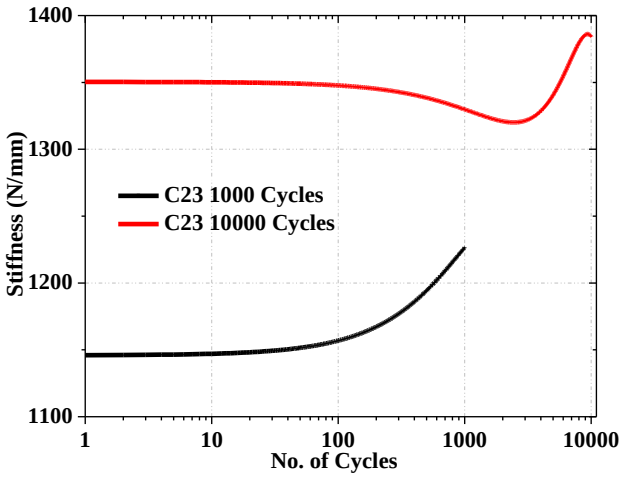

Figure 20: Average stiffness for 3rd set of segments *Figure 21: Stiffness for segment tested w/o pure moment*

The final segment was tested in saline bath without the pure moment, and the segment responded with a limited change in axial stiffness during the first 1,000-cycle set and limited change (10%) between the 1,000 and 10,000 cycle sets. Based on the findings, the testing protocol was adjusted to limit pure moment testing between fatigue sets, while maintaining the saline bath for all fatigue cycles. Specimens fatigue tested in saline demonstrated a modest change in stiffness (4%) during the first 1,000 cycles, which is more in line with expectations. However, specimens tested without saline demonstrated over a 20% change in stiffness during the first 1,000 cycles. Likewise, exclusion of the pure moment protocol resulted in limited test-to-test changes (13%) between 1,000 and 10,000 cycles. When testing included the pure moment protocol, mean test-to-test changes were somewhat greater (15%).

Part 2: As observed during the tests of previous quarter the compressive displacement required to achieve 150N for the segments was reduced with increasing number of fatigue cycles. It can be observed that the relative strain decreased with respect to the number of cycles and was observed to be between 1-4% (Figure 22) for all the segments tested up to 50,000 cycles. It can be observed that the relative strain curve behavior did not change a lot for the first and second fatigue set, except the initial strain was more during first fatigue set as compared to second. The absolute strain of the segments was observed to increase up to 10-20% (Figure 23), suggesting that there is about 8 to 18% residual strain in the segments. The absolute strain was observed to be a function of number of applied cycles for first 10,000 cycles, whereas the slope of the absolute strain is observed to be almost constant for each interval of 10,000 cycles. As the segments were allowed to relax after the fatigue test, it was observed to regain some of its lost height and the residual strain was reduced. However the segments never regained their original heights.

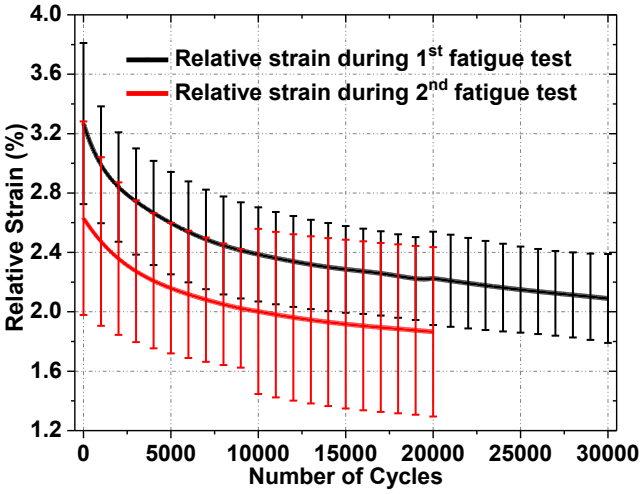

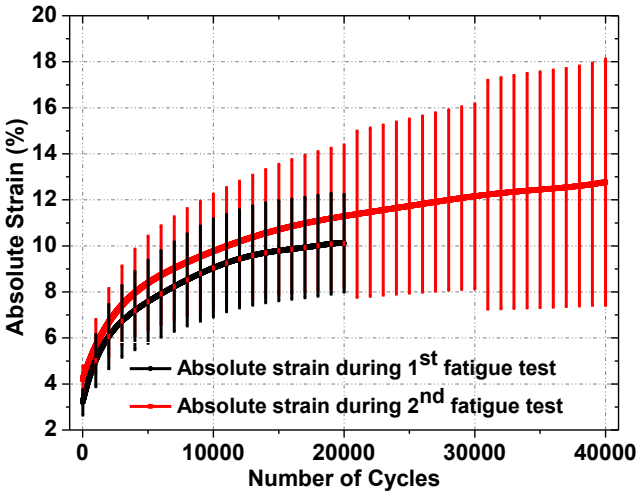

Figure 22: Relative strain response of the segments *Figure 23: Absolute strain response of the segments*

The stress relaxation response in terms of stress with respect to time showed that before any fatigue the segment showed least stress for the strain. But further for the same amount of strain the stress in the segment after the fatigue tests was observed to increase (Figure 24). It was observed that after the second fatigue test, the stress was considerably higher; suggesting that the fatigue test stiffened the segment. The asymptote of the curve was also shifted and took more time

to show the steady response. After first and second fatigue tests pure moment test was performed on each segment in flexion extension and lateral bending at 0.3, 0.5, 1, 1.5 and 2Nm. After the first fatigue test the range of motion of the segments is on higher side as compared to Wheeldon et al. 2006 (Figure 25). The average increase in the range of motion between the first and second fatigue cycle is about 28% in flexion.

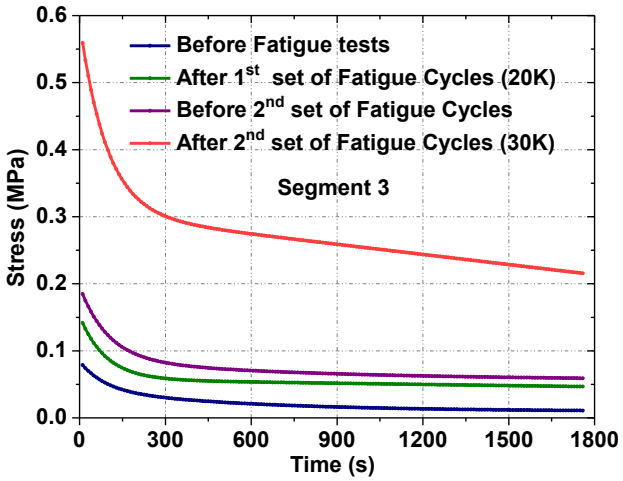

Figure 24: Viscoelastic response for segment 3 before and after fatigue test

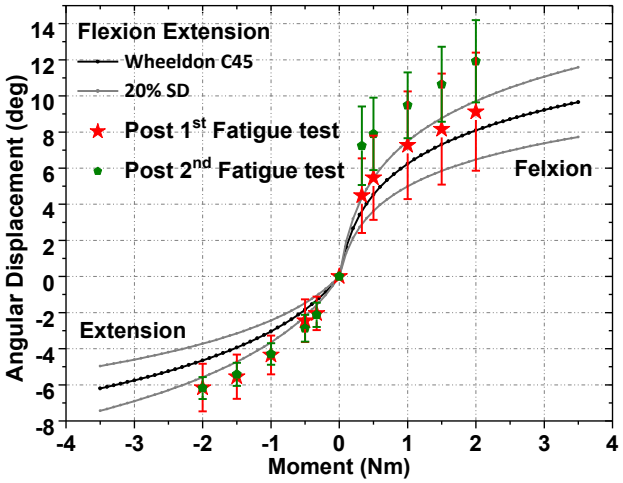

Figure 25: Pure Moment response of in flexion and extension.

The heights of the discs were also measured from the x-rays and averages of three measurements were taken at right, left and center of the IVD and the average was taken. The average and percentage change in the disc heights are tabulated in Figure 18. The percentage change in disc height was observed to be comparable with absolute strain, except segment 3 which showed more decrease in height. It was perhaps due to error in height measurement or injury which would be clear from MRI scans. The disc heights are reduced mainly due to dehydration of the soft tissue and if the tissue is allowed to relax in a water bath it again regains its height up to a certain extent.

Table 7: Heights of the segments before and after fatigue tests

S. N.	Initial Height (mm)	Cycles Set 1	Height After 1st	Decrease %	Cycle Set 2	Height After 2nd	Decrease %

			fatigue set			fatigue set	
1	9.824	10000	9.123	7.14	40000	7.437	18.48
2	9.809	10000	9.336	4.82	40000	8.97	3.92
3	9.457	20000	9.071	4.08	30000	6.596	27.28
4	8.404	30000	7.207	14.24	20000	6.962	3.39
5	7.485	10000	6.399	14.51	40000	5.579	12.81

It was difficult to compare results with sets having different fatigue cycles. So in the next set of experiments removal of the segment form the water was designed to be avoided. Also, in the next experimental protocol posterior elements were removed and all the tests were performed in a flow and without removing the segment for the saline bath.

Part 3: In the resent set of experiments four segments were tested under a cyclic compressive force of 0-150N at 2Hz up to 50,000 cycles at an interval of 10,000 cycles. The force cyclic response for one of the segments for 10,000 cycles is plotted in Figure 26, whereas the zoomed-in image shows the force plot with respect to time for two cycles. The force response of all the segments was observed to be smooth sine wave with no abnormal peak or trough, which would suggest damage to segment.

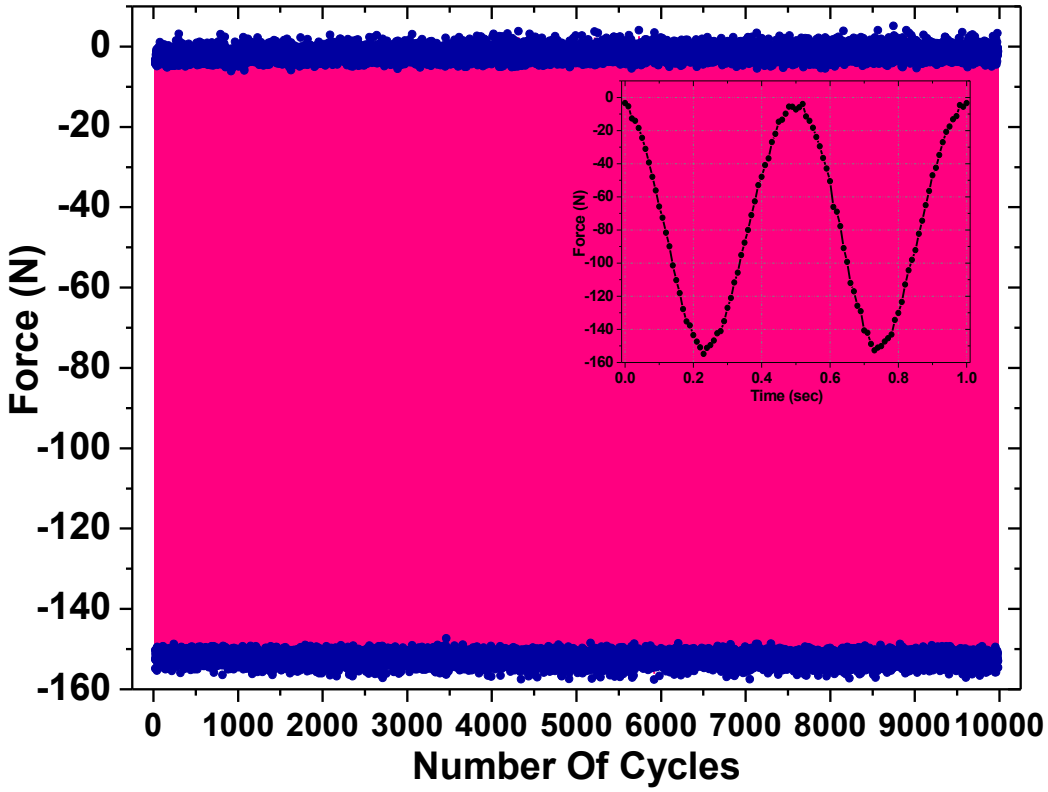

Figure 26: Cyclic force response of the segment

It was observed that the absolute strain i.e. the strain with respect to the initial height of the disc, during fatigue increased with an increasing number of fatigue cycles. The absolute strain and the height with respect to each cycle was calculated for all four segments and is plotted in Figure 27. It can be observed that the absolute strain and / or the disc height loss, was maximum during the first 10,000 cycle fatigue set. As the number of cycles increased, the IVD demonstrated a more stable response and the absolute strain during the fourth and fifth fatigue set was almost identical. For segment 2 it was observed that during the third fatigue set there was a sudden increase in absolute strain or decrease in height, which represents that there must have been some failure and it is also validated by the viscoelastic test which shows sudden increase in force post third fatigue set. Results for testing of that segment were only included up to the time of failure. Dissection of that segment is currently planned and will detail specific structures that failed during the fatigue loading. Segment 4 was the only exception to this behavior of gradual drop in absolute strain curves and showed increase during second, third and fourth fatigue sets. The average curves of

absolute strain and height loss for all the segments (last figure in Figure 27) clearly shows the difference between the fatigue sets. As the segments were allowed to relax after the fatigue test, it was observed to regain some of its lost height and the residual strain was reduced. However the segments never regained their original heights (Table 8).

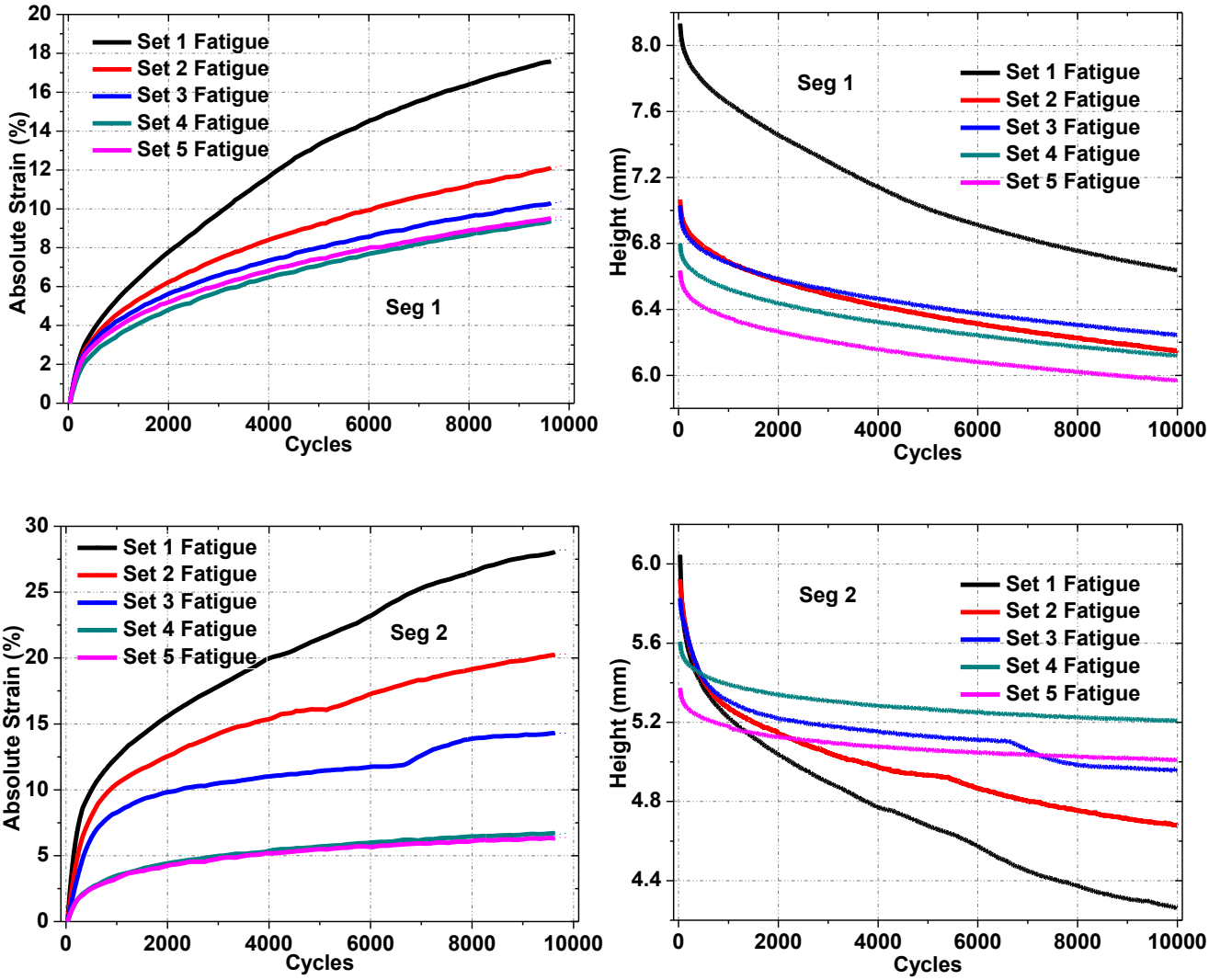

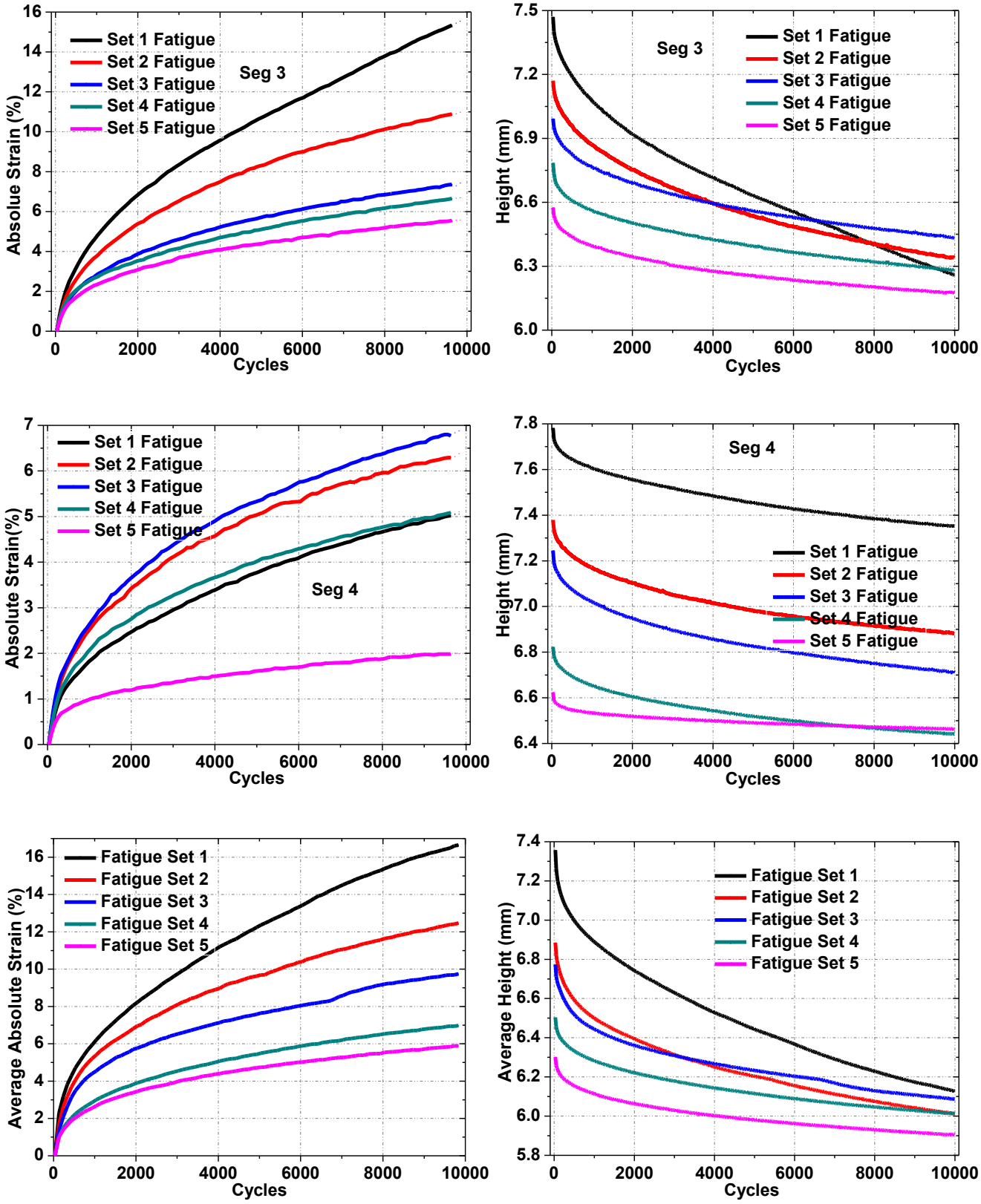

Figure 27: Absolute strain and decrease in height response of the segment

Intervertebral disc heights were measured from the x-rays before and after the fatigue tests. Averages of three measurements were taken at right, left and center of the IVD. The average and percentage disc height losses are tabulated in Table 8. Disc height loss was maximum during the first fatigue set averaging 5.5%. The height loss further reduced with the fatigue sets and there was least difference post fourth and fifth fatigue set disc height. The average disc height loss between set 1 and set 5 i.e. after 50,000 cycles is obtained as 14%, with 18% maximum for the segment 1 and 11% minimum for segment 2. It can also be observed from average height loss in Figure 27 that the curve profile for first two fatigue sets is similar and the curve profile for next three fatigue sets is similar. It shows that for the first two fatigue sets the disc demonstrates viscoelastic properties, whereas for the next three sets the disc shows only elastic response with decrease in height. The disc heights are reduced mainly due to dehydration of the soft tissue and if the tissue is allowed to relax in the water bath it again regains its height up to a certain extent. Thus if a considerable permanent change in disc height is obtained it can be used as failure parameter, however that percentage needs to be determined with more experiments.

Table 8: Heights of the segments before and after fatigue tests

	Seg1	Loss (%)	Seg2	Loss (%)	Seg3	Loss (%)	Seg 4	Loss (%)	Avg Loss (%)
Initial	8.13		6.05		7.47		7.78		
Post Fatigue 1	7.07	0.13	5.92	0.021	7.35	0.016	7.38	0.05	0.055
Post Fatigue 2	7.03	0.006	5.83	0.015	7.17	0.024	7.24	0.02	0.016
Post Fatigue 3	6.8	0.033	5.6	0.04	6.99	0.025	7	0.033	0.033
Post Fatigue 4	6.65	0.022	5.37	0.04	6.78	0.030	6.82	0.026	0.03
Post Fatigue 5	6.64	0.0015	5.37	0	6.57	0.030	6.62	0.03	0.015
		0.18		0.11		0.12		0.15	0.14

Viscoelasticity: Before first and after each fatigue set a stress relaxation viscoelastic test was performed on each segment and quasi linear viscoelastic material parameters were extracted for each using equation (6). The parameters were optimized with the experimental curve using a

Matlab function *fminsearch*. The stress relaxation response in terms of stress with respect to time is plotted in Figure 28. It can be observed that for segment 2 and 4, before any fatigue the segment showed least stress for the strain caused by 10% strain load, but further for the same amount of strain the stress in the segment after the fatigue two fatigue sets was observed to increase, whereas segment 1 and segment 3 showed mixed behavior. The asymptote of the curve is also shifted and takes more time to show the steady response.

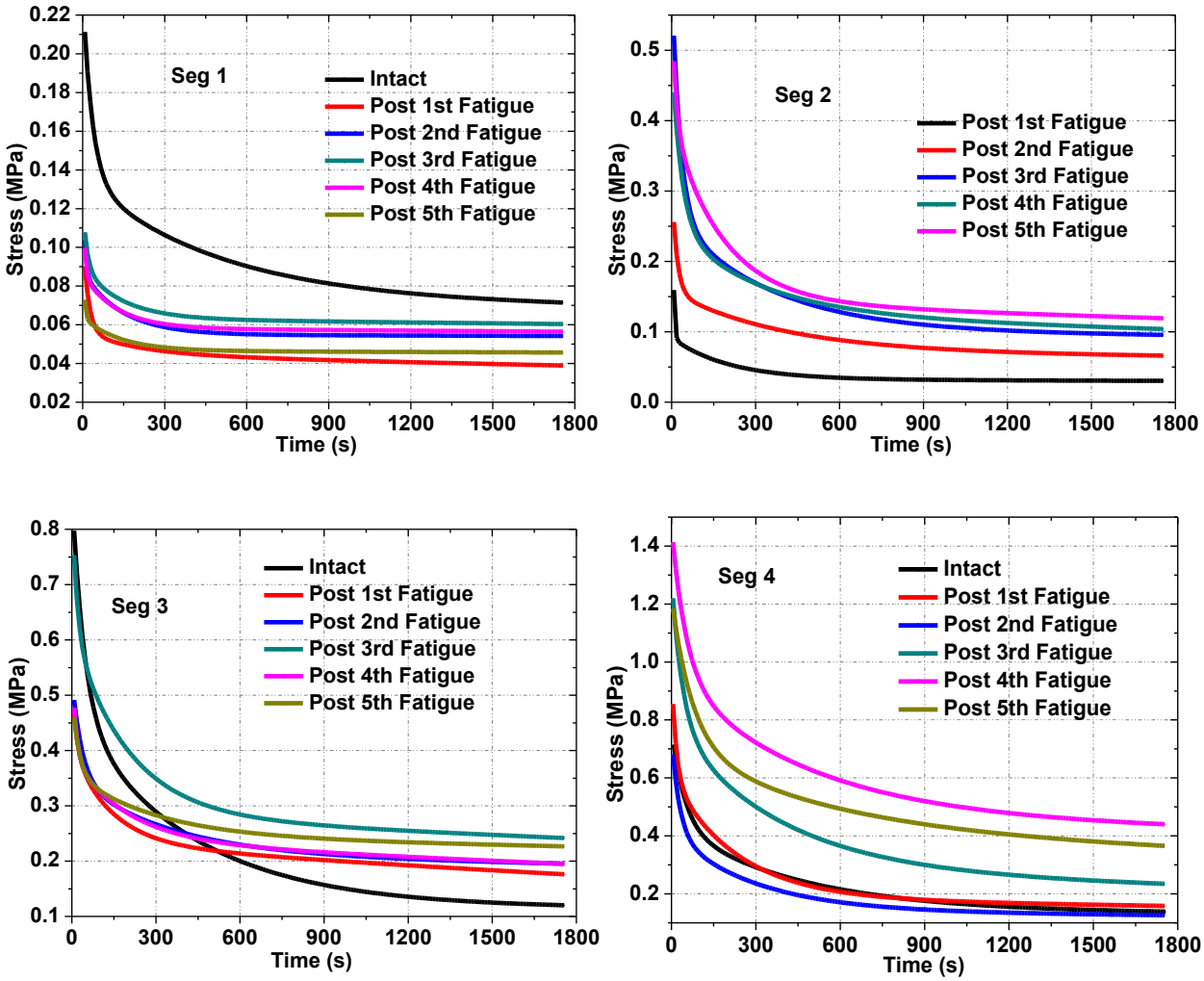

Figure 28: Viscoelastic response for all segments after fatigue sets

The quasi-linear viscoelastic material parameters for all the tests are tabulated in Table 9. It can be observed from Table 9 that the stress response constants A and B are observed to increase after the fatigue test whereas the relaxation constants (a, b, c, d, g & h) are observed to decrease with a couple of exceptions due to experimental results. It denotes that the relaxation constants

work over a time interval. Constants a & b represent the initial slope of the curve or the first time interval c & d represent the second, whereas g & h represent the later part of the curve. Thus it can be inferred that the increase in stiffness constants and decrease in the relaxation constants show the stiffening of the intervertebral disc, and the change in the time relaxation constants result in shifting of the asymptote.

Table 9: Quasi Linear Viscoelastic parameters before and after fatigue tests

SN	Fatigue	Quasi Linear Viscoelastic Material Parameters							
		A	B	a	b	c	d	g	h
Seg 1	Intact	0.0086	9.34	0.24	0.03	0.18	0.002	0.22	3.17E-05
	Post 1st Set	0.045	8.96	0.035	0.052	0.01	0.005	0.04	7.67E-05
	Post 2nd Set	0.008	8.95	0.143	0.16	0.15	0.007	0.266	7.12E-06
	Post 3rd Set	0.0067	8.98	0.13	0.069	0.14	0.007	0.34	2.49E-05
	Post 4th Set	0.015	8.6	0.096	0.16	0.106	0.008	0.23	1.76E-05
	Post 5th Set	0.025	7.95	0.087	0.21	0.075	0.0073	0.21	1.07E-05
Seg 2	Intact								
	Post 1st Set	0.01	9.93	0.14	0.06	0.098	0.0025	0.084	5.71E-05
	Post 2nd Set	0.02	10.086	0.2	0.034	0.11	0.003	0.07	3.65E-05
	Post 3rd Set	0.028	9.37	0.22	0.03	0.13	0.003	0.13	0.00011
	Post 4th Set	0.0025	12.9	0.046	0.067	0.097	0.005	0.056	0.000103
	Post 5th Set	0.01	10.8	0.082	0.28	0.03	0.005	0.017	3.77E-05
Seg 3	Intact	0.029	9.61	0.166	0.023	0.16	0.0024	0.0554	1.68E-05
	Post 1st Set	0.04	8.94	0.11	0.02	0.074	0.002	0.12	2.13E-05
	Post 2nd Set	0.02	8.99	0.22	0.029	0.19	0.0023	0.3	5.09E-05
	Post 3rd Set	0.01	10.84	0.072	0.059	0.13	0.005	0.11	9.01E-05
	Post 4th Set	0.012	9.35	0.17	0.07	0.22	0.005	0.35	0.00011
	Post 5th Set	0.015	9.45	0.12	0.044	0.12	0.003	0.25	4.60E-05
Seg 4	Intact	0.024	10.89	0.12	0.022	0.12	0.0022	0.06	3.96E-05
	Post 1st Set	0.0003	15.58	0.1	0.0622	0.17	0.0043	0.077	9.01E-05
	Post 2nd Set	0.026	8.82	0.9	0.036	0.86	0.0033	0.46	6.51E-05
	Post 3rd Set	0.01	12.272	0.23	0.026	0.26	0.0026	0.15	1.14E-04
	Post 4th Set	0.003	13.92	0.2	0.02	0.2	0.0021	0.2	5.01E-05
	Post 5th Set	0.05	10.662	0.23	0.013	0.15	0.0018	0.2	9.29E-05

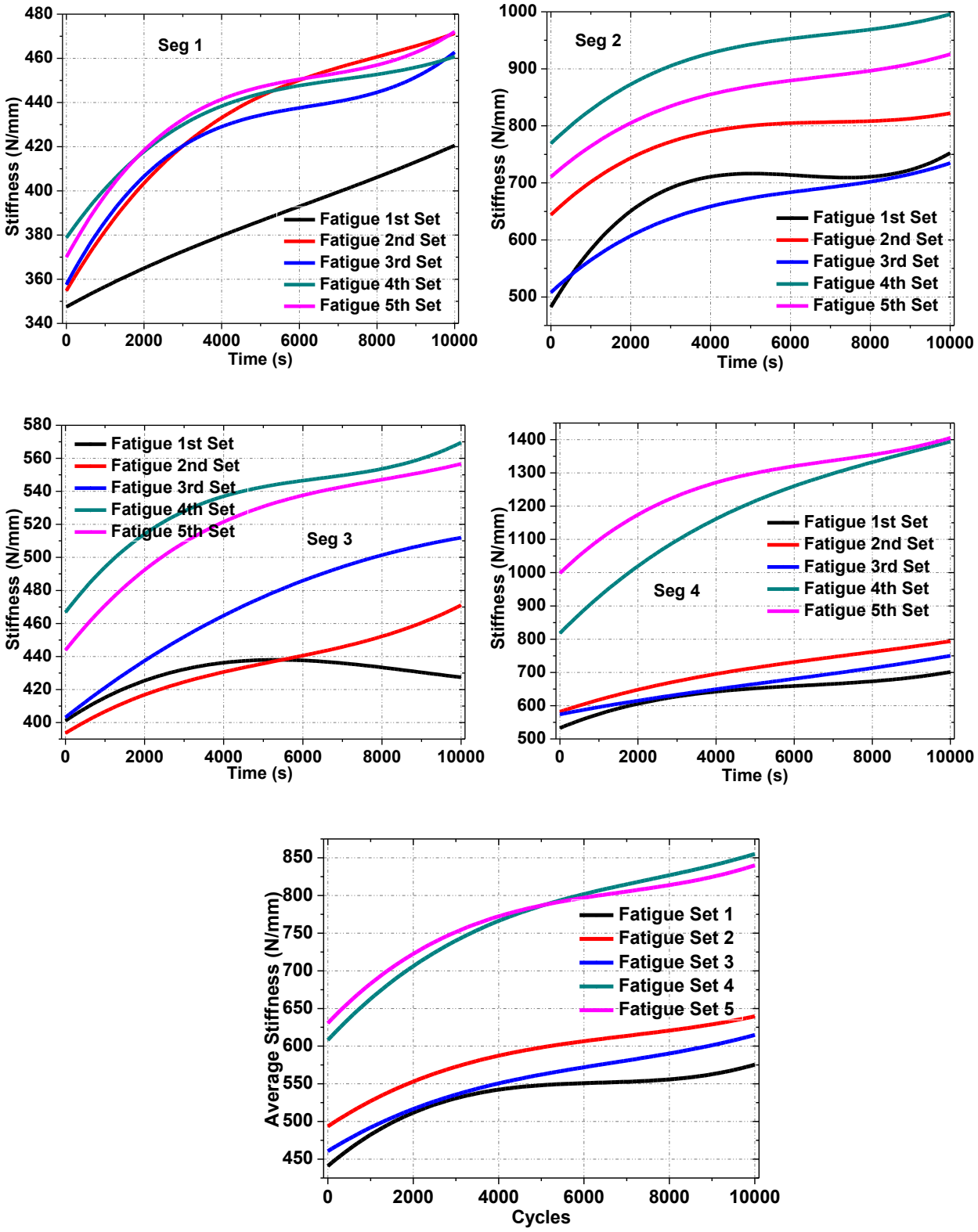

Figure 29: Stiffness response for all segments during fatigue sets.

Stiffness: The increase in stiffness for the four disc segments and average stiffness for all the segments during fatigue is illustrated in Figure 29. It can be observed that during first three sets

there was not much change in stiffness of the disc, whereas fourth and fifth sets showed a high increase in stiffness. This behavior is observed due to decrease in disc height and loss in viscous behavior. Loss in viscosity can also lead to functional losses and thus failure of the soft tissue.

Tension Compression: The tension and compression curves from the tests along with average curves are shown in Figure 30. It can be observed that the discs showed less stiff behavior in tension with increase in fatigue, whereas it shows stiffer behavior in compression. Again this behavior was observed due to decrease in disc height and loss in viscous behavior. The behavior could also be indicative of progressive yielding-type behavior of the annular fibers (Stemper et al. 2014) , resulting in annular laxity. Increased annular laxity could contribute to lost disc height and would have a mechanical signature of decreased tension stiffness as the laxity is taken up in during the early stages of tension, and increased compressive stiffness, as the decreased disc height results in more bulk mass of the disc resisting compression earlier in the compressive response. The tension compression results will be converted to stress strain plots and will be fitted with desired material models to obtain material parameters which will be used for updating the finite element model.

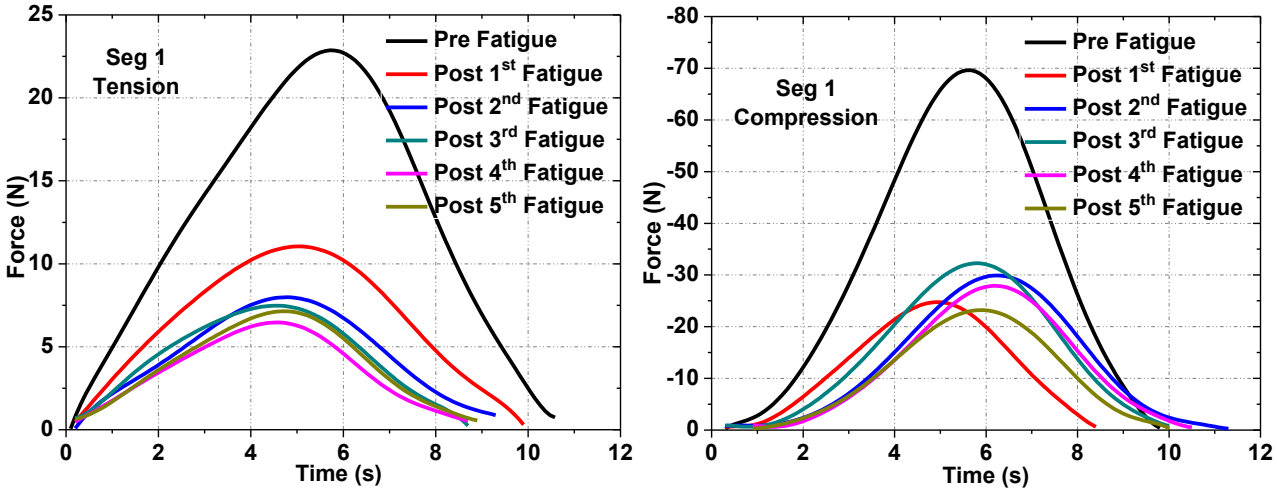

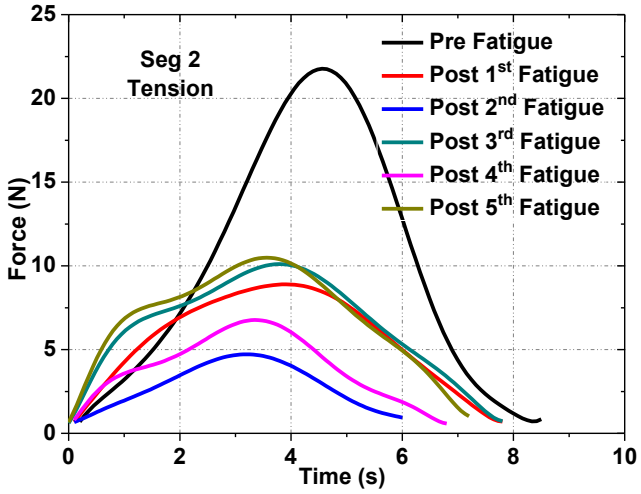
Seg 2
Tension
Pre Fatigue
Post 1st Fatigue
Post 2nd Fatigue
Post 3rd Fatigue
Post 4th Fatigue
Post 5th Fatigue
Force (N)
Time (s)

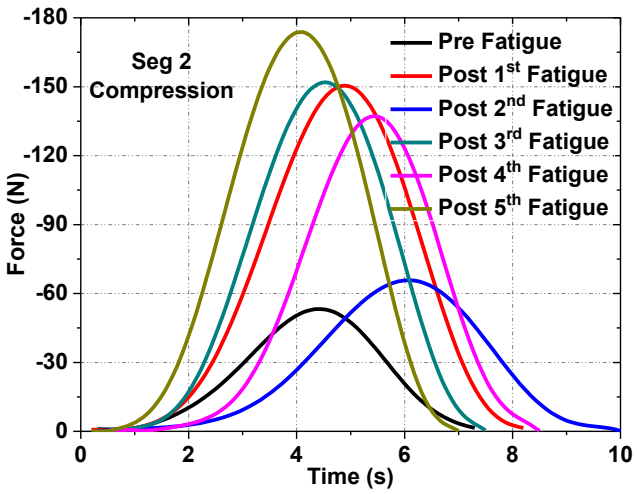
Seg 2
Compression
Pre Fatigue
Post 1st Fatigue
Post 2nd Fatigue
Post 3rd Fatigue
Post 4th Fatigue
Post 5th Fatigue
Force (N)
Time (s)

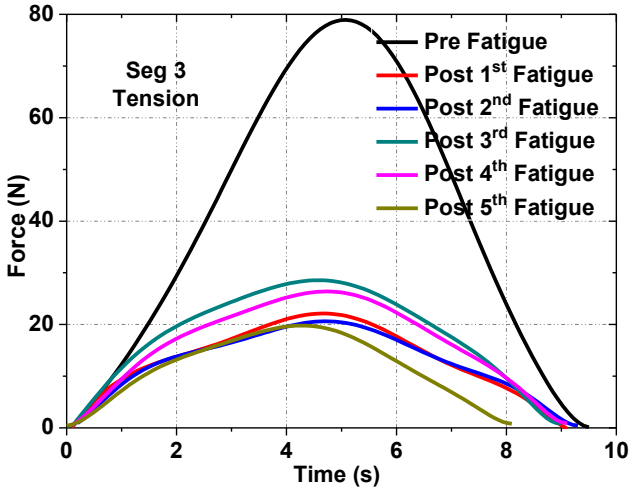
Seg 3
Tension
Pre Fatigue
Post 1st Fatigue
Post 2nd Fatigue
Post 3rd Fatigue
Post 4th Fatigue
Post 5th Fatigue
Force (N)
Time (s)

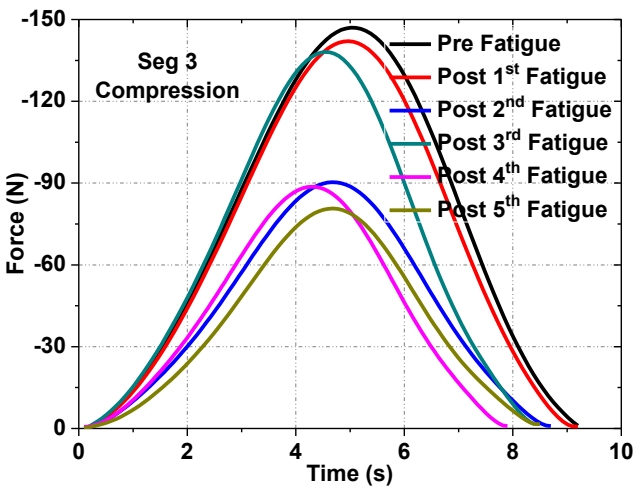
Seg 3
Compression
Pre Fatigue
Post 1st Fatigue
Post 2nd Fatigue
Post 3rd Fatigue
Post 4th Fatigue
Post 5th Fatigue
Force (N)
Time (s)

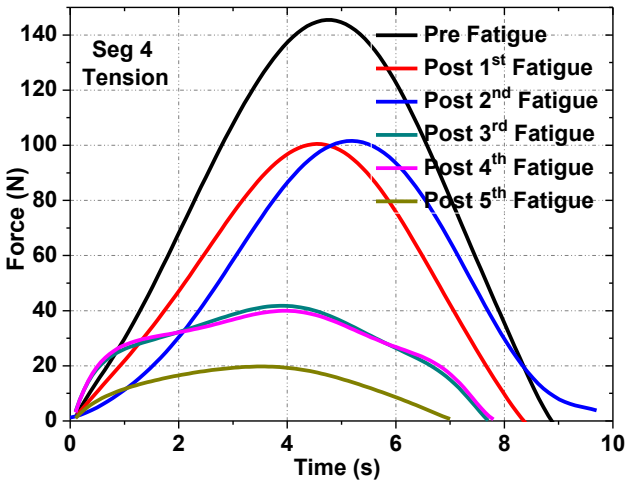
Seg 4
Tension
Pre Fatigue
Post 1st Fatigue
Post 2nd Fatigue
Post 3rd Fatigue
Post 4th Fatigue
Post 5th Fatigue
Force (N)
Time (s)

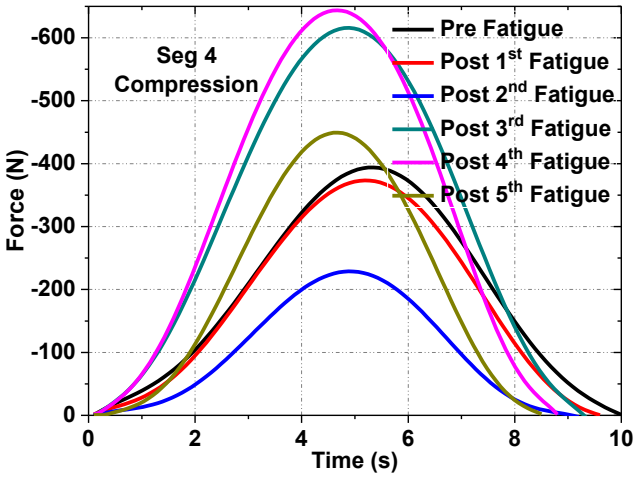
Seg 4
Compression
Pre Fatigue
Post 1st Fatigue
Post 2nd Fatigue
Post 3rd Fatigue
Post 4th Fatigue
Post 5th Fatigue
Force (N)
Time (s)

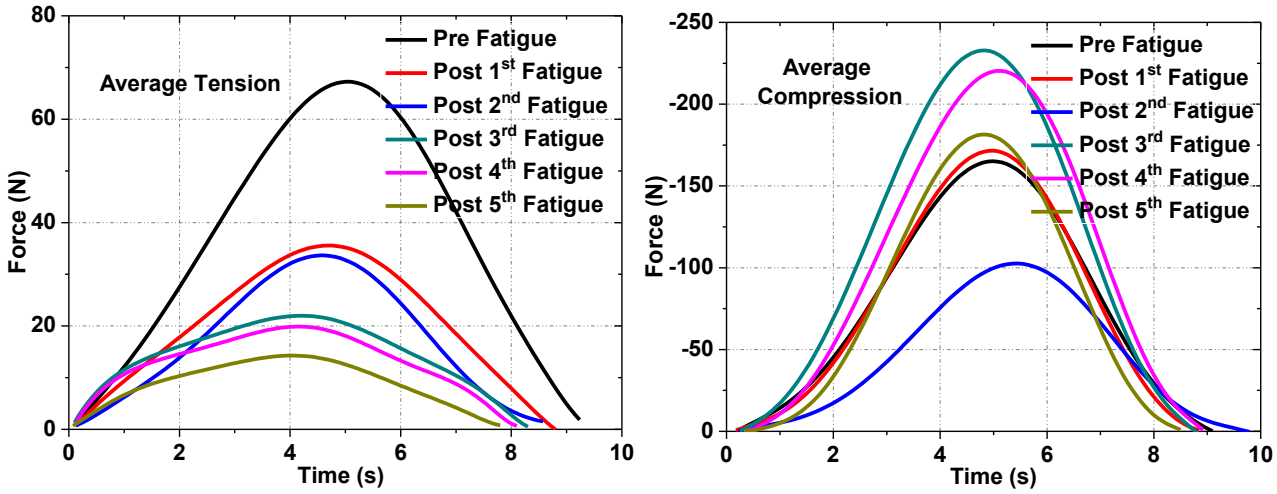

Figure 30: Tension Compression response for all segments post fatigue sets.

Finite Element Modeling

Finite element modeling of soft tissues under fatigue is a very difficult task and it has never been done before. During this study various attempts were made to develop a finite element model which could replicate fatigue. The efforts of finite element modeling are also divided in three parts as follows.

Part 1: In the first attempt, a finite element model of the spine segment in LS Dyna was obtained and a freshly implemented module in LS Dyna was used (*FREQUENCY_DOMAIN_RANDOM_VIBRATION) which incorporates location, direction and range of frequencies for the random excitation, exposure time and SN curve. As per experiments, cyclic load was applied to the spine segment as shown in Figure 31, for segment C67, all the surface nodes of vertebra C7 were constrained in x, y and z direction and a cyclic load of 150N was applied on the cortical bone of C6. LS dyna performs modal analysis as the first step and the natural frequencies and the mode shapes were determined. Based on all the above data LS Dyna determines cumulative damage ratio, expected fatigue life and irregularity factor as the fatigue parameters. While defining the boundary conditions for fatigue, the loading was defined in the frequency domain (PSD- power spectral density). Therefore, the FFT of the force-time curve was calculated and the load was applied in frequency domain as PSD. The frequency range for

the modal analysis as well as the number of mode over which fatigue will be distributed has to be defined.

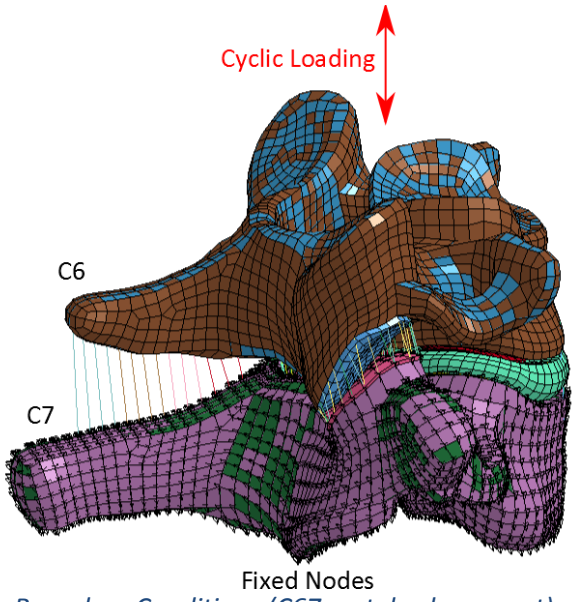

Figure 31: Boundary Conditions (C67 vertebral segment)

The results were obtained in terms of mode shapes and natural frequencies for the segment C67. The mode shapes for the lower frequencies were the normal modes such as flexion-extension, bending and rotation. However for higher frequencies the intervertebral disc showed unrealistic mode shapes, in which the disc deformed to such an extent that it penetrated into the vertebral bone, making the model unstable for higher frequencies.

To correct that, the material properties and the boundary between the parts (nucleus, annulus, annulus fibrosus and the endplates) had to be modified. And it was discovered that only high strength material can be used for this kind of analysis in LS Dyna. Soft issues or hyper elastic materials are unable to replicated fatigue using this method in LS Dyna.

Part 2: Further, another software 'n code' (HBM-nCode Inc., Southfield, MI) was used to determine fatigue in discs. N-code is software which is developed for industrial fatigue analysis applications. It accepts material properties (Elastic Modulus, Poisson's ratio, Yield Stress etc.) and fatigue properties in terms of SN or EN Curve are generated from them. A loading simulation analysis for unit load has to be provided from the Finite Element software (LS Dyna in our case). The loading conditions (random vibrations or sinusoidal vibration), number of loading cycles and

loading force can be adjusted in N-code, and the output is obtained as damage sustained and life of the object. So, the segment C4-C5 was separated from the spine model and the boundary conditions were applied as in the experiments. The inferior vertebra (C5) was fixed and the superior vertebra (C4) was applied with a sinusoidal force of 1N for 0.5s (1 cycle). The result of the FE simulation was used as input in the n code for fatigue analysis.

The snapshot of glyphs used for fatigue analysis is shown in Figure 32. The FE Input glyph represents the result of FE simulation (unit compressive load in 0.5sec), the second glyph 'EN analysis' performs the EN analysis and thus requires EN curve for each part on which fatigue analysis has to be performed. The n-code software is meant for the fatigue analysis of metals, and the SN or EN curve is developed for each part from the material properties of the part. Hence only the material properties of only the IVD were used as obtained from the experiments (Elastic Modulus = 10MPa and Poisson's ratio=0.45). The third glyph shows the output of the fatigue analysis in terms of 'damage' and 'life' of the material which are inversely equal.

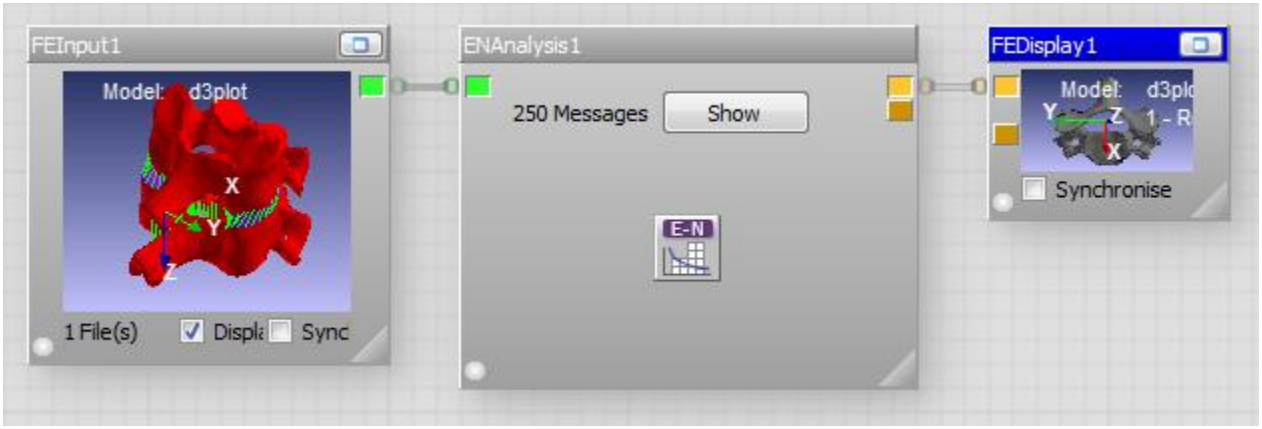

Figure 32: Glyph snapshot of n-code used for fatigue analysis

The analysis was performed for 50000 cycles at a compressive force of 150N. The damage and life observed for IVD (Inter vertebral disc) is plotted in Figure 33. It wasobserved that for the loading condition, the life interpreted for IVD is interpreted more than 6E7 cycles; the damage is observed to be very small at the inferior end of the disc. Also during the experiments, the segments didn't show any visible damage after 50000 fatigue cycles. Further the fatigue analysis was performed in n-code with higher force and the life contour plots for the IVD are shown in Figure

34 and Figure 35 for 500N and 1000N force. It was observed that with increase in force, the life of the tissue is observed to reduce to 2146 cycles and 190 cycles for 500N and 1000N force respectively. As compared to literature these values were too small.

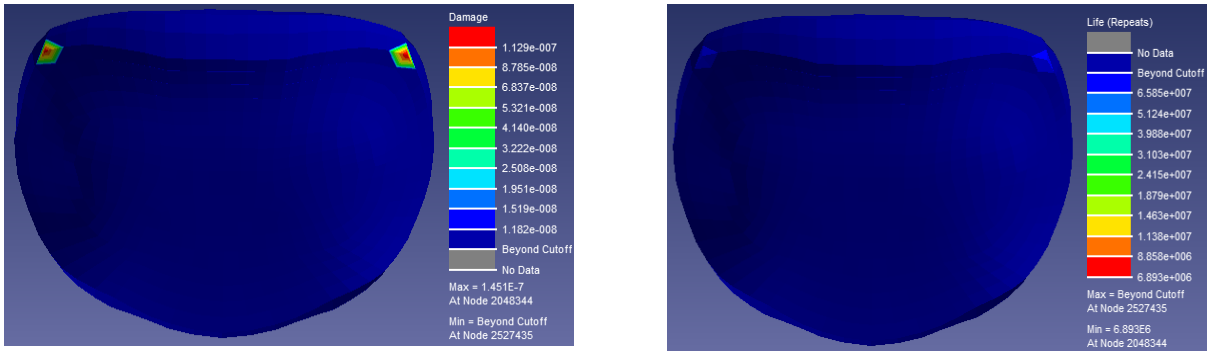

Figure 33: Damage and Life of the IVD for 50000 cycles and 150N force

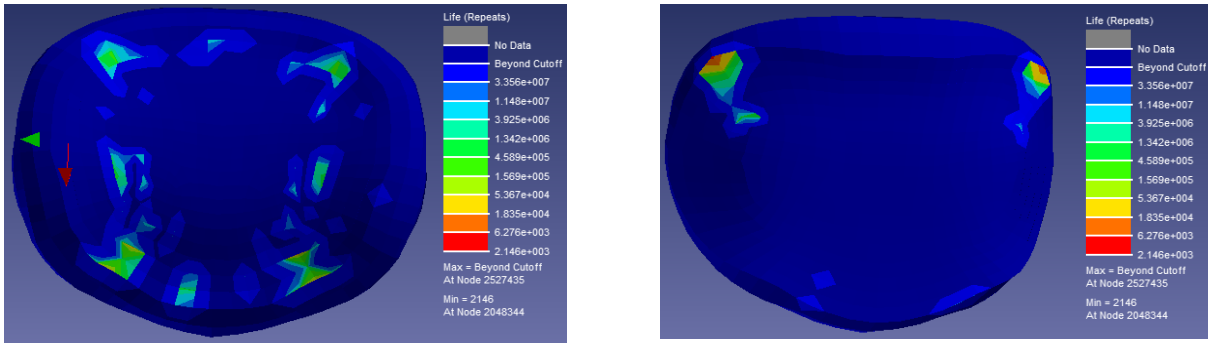

Figure 34: Life of the IVD for 50000 cycles and 500N force

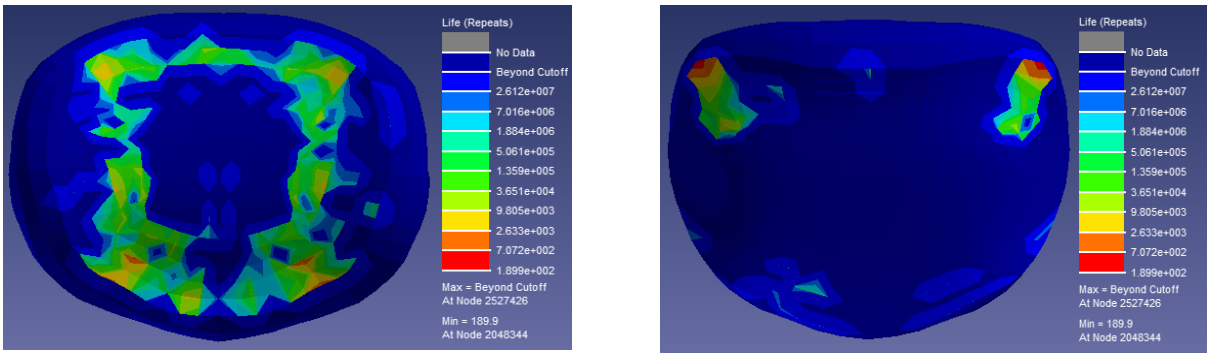

Figure 35: Life of the IVD for 50000 cycles and 1000N force

The superior side of the discs was observed to have more damage as compared to the inferior side. Though the model showed exponential decrease in life with increase in the load, the

software is built for to predict the fatigue in metals and the potential of it to produce fatigue in soft tissue accurately is still questionable. Also for this case the fatigue with higher force will have to be investigated experimentally. Hence, though n code represented some kind of fatigue in the soft tissue, it still needs better understanding and experimental validation to correctly predict the life of intervertebral disc.

Part 3: For recent protocol, the finite element model was obtained as discussed in previously. The elements were further renumbered so that all the parts have serial element Ids. A Matlab algorithm was further developed to note the ids of nucleus and annulus and material ids with the same id as that of part ids were created. The material ids were then referred to the corresponding element id and the discretized model for disc was created. The Figure 36 shows the finite element model with annulus and nucleus modeled with discrete parts. The model was applied with boundary conditions and loading.

Another Matlab algorithm was developed, which can execute the model in loop and read the results and update the model after a corresponding execution. To illustrate, once the first execution is done the algorithm will read through the von mises stress output file. The elements with more than average stress will be sorted out and the material properties for those elements will be updated from a lookup file which will be based on the material properties calculated from tension compression tests during fatigue. The final fatigue simulation will show the elements with most stress and degraded material properties. The objective here will be to develop a material data base for degraded material properties of disc and determining the location is highest stress or failure using those material properties. The assumption made here is that the one cycle simulation in LS Dyna demonstrates same results as of 10,000 cycles experimentally. This is done as time required for each simulation is more than 10 hours and increasing the number of cycles will increase the simulation time considerably. The simulations are being done and the results will be provided in the next deliverable.

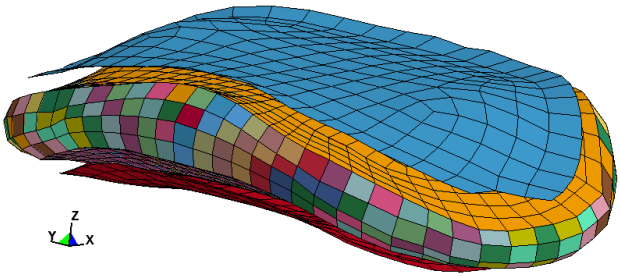

Figure 36: FE model of cervical spine intervertebral disc with different material for each annulus element.

4. REPORTABLE OUTCOME

4.1 Conference Presentation

Ultrasound Can Measure Dynamic Motion of Cervical Spine Intervertebral Disc, Orthopaedics Research Society 2013 (Poster)

Clinical Ultrasound Can Measure Dynamic Intervertebral Disc Deformation In-vivo, Orthopaedics Research Society 2013 (Poster)

Real-Time Ultrasound Can Measure Dynamic Properties of Cervical Spine Intervertebral Disc, Orthopaedics Research Society 2014 (Conference Poster)

3D Kinematics Using Dual Ultrasound Stereographic Imaging of Human Cervical Spine, Aerospace Medical Association (Conference Oral Presentation)

Ultrasound Imaging of Cervical Spine Intervertebral Discs, 2014 World Congress of Biomechanics

Use of Portable Ultrasound to Measure Dynamic Motion of Cervical Spine Ex-Vivo and In-Vivo, Biomedical Engineering Society 2014 (Conference Oral Presentation)

Dual Ultrasound Can Measure Kinematic Motion and Intervertebral Disc Deformation of Cervical Spine, Orthopaedics Research Society 2015 (accepted as Conference Poster)

Dynamic Ultrasound Imaging of Cervical Spine Intervertebral Discs, 2013 IEEE International Ultrasonics Symposium (Poster)

Dynamic Ultrasound Imaging of Cervical Spine Intervertebral Discs, 2014 IEEE International Ultrasonics Symposium (Conference Oral Presentation)

4.2 Publication

Zheng M, Shiuan K, Masoudi A, Buckland D, Szabo T, Snyder B: Dynamic ultrasound imaging of cervical spine intervertebral discs, Ultrasonics Symposium (IUS), 2013 IEEE International, Page(s): 836-839

Zheng M, Masoudi A, Buckland D, Stemper B, Yoganandan N, Szabo T, Snyder B: Dynamic ultrasound imaging of cervical spine intervertebral discs, Ultrasonics Symposium (IUS), 2014 IEEE International, Page(s): 448-451

Umale S, Stemper BD, Zheng M, Masoudi A, Fama D, Yoganandan N, Snyder BD. Methodology to calibrate disc degeneration in the cervical spine during cyclic fatigue loading. Biomed Sci Instrum (in review).

Umale S, Stemper BD, Zheng M, Masoudi A, Fama D, Yoganandan N, Snyder B: Progressive changes in cervical spine intervertebral disc properties during cyclic compressive fatigue loading. ASME Summer Biomechanics, Bioengineering, and Biotransport Conference, Snowbird Resort, Utah, June 17-20, 2015 (in review).

Umale S, Stemper BD, Zheng M, Masoudi A, Yoganandan N, Snyder BD. Changes in cervical intervertebral disc viscoelasticity during repetitive axial loading: A preliminary report. 2015 Annual Meeting of the Orthopedic Research Society, Las Vegas, NV, March 28-31, 2015.

4.3 Provisional Patent Claim

Imaging of Multiple Projection Ultrasound System to measure structural kinematics in human

An ultrasound system complex, comprising:

1. multiple ultrasound systems synchronized for simultaneous acoustic imaging data acquisition
2. stereoscopic transducer positioning through mechanical means and/or positioning sensors
3. dynamic displacement tracking in 3D (3 coordinates) of imaged objects based on raw radio frequency data from each imaging system
4. high resolution long term tracking low error achieved through specialized tracking algorithms

5. CONCLUSION

We have developed a dual ultrasound system can be used to non-invasively measure IVD deformation and mechanical compliance *ex-vivo*, and provide real-time images of IVDs and dynamic vertebral motion *in-vivo* during simulated tasks relevant to acute and chronic cervical spine injury and disease. Software was developed to track the motion of a user-specified region of interest that corresponds to the anterior and posterior bony profiles of cervical vertebrae. For motion frequencies up to 8Hz, US accounted for 95% of the true IVD displacements and the estimated error was 0.06mm. In our preliminary experiments using the dual US system *ex-vivo and in-vivo,* we studied the dependence of the compliance of IVD measured directly vs. the subjects' age and Pfirrmann Grade measured by MRI. The "quality" and hydration of the IVD affected the measured compliance, while the damping coefficient was unaffected. The IVD/FSU for younger specimen/subject tends to be more compliant in creep test analysis compared to older specimen/subject. To achieve more reliable measurement of IVD properties *in-vivo*, a diagnostic system was developed that safely applies dynamic cyclic loads to cervical spine over a range of programmable frequencies and amplitudes that simulate operational conditions.

In C-spine modeling, it was observed that the experimental conditions during fatigue testing affect outcomes drastically; soft tissues become dehydrated quickly under ambient conditions that are ameliorated by using a saline bath. The results from C-spine cyclic loading were used to generate material parameters which were incorporated into the FE model for IVD fatigue. Matlab algorithms were developed to discretize the FE model of the IVD so that changes in the material properties of the nucleus and annulus elements as a function of number of applied load cycles were updated during the fatigue test FE analysis to reflect progressive deterioration of their material properties obtained from the fatigue experiments.

6. REFERENCE

Rahimi A, Morency L-P. 2001. "Reducing drift in parametric motion tracking." Computer Vision, 2001. ICCV 2001. Proceedings. Eighth IEEE International Conference on. Vol. 1. IEEE, Abramowitch, Steven D. 2004. “An Improved Method to Analyze the Stress Relaxation of Ligaments Following a Finite Ramp Time Based on the Quasi-Linear Viscoelastic Theory.” Journal of Biomechanical Engineering 126 (1): 92.

Qasim, Muhammad, Raghu N. Natarajan, Howard S. An, and Gunnar B.J. Andersson. 2012. “Initiation and Progression of Mechanical Damage in the Intervertebral Disc under Cyclic Loading Using Continuum Damage Mechanics Methodology: A Finite Element Study.” Journal of Biomechanics 45 (11): 1934–40.

Qasim, Muhammad, Raghu N. Natarajan, Howard S. An, and Gunnar B.J. Andersson. 2014. “Damage Accumulation Location under Cyclic Loading in the Lumbar Disc Shifts from Inner Annulus Lamellae to Peripheral Annulus with Increasing Disc Degeneration.” Journal of Biomechanics 47 (1): 24–31..

Stemper, Brian D., Jamie L. Baisden, Narayan Yoganandan, Barry S. Shender, and Dennis J. Maiman. 2014. “Mechanical Yield of the Lumbar Annulus: A Possible Contributor to Instability: Laboratory Investigation.” Journal of Neurosurgery: Spine 21 (4): 608–13.

Toms, Stephanie R., Greg J. Dakin, Jack E. Lemons, and Alan W. Eberhardt. 2002. “Quasi-Linear Viscoelastic Behavior of the Human Periodontal Ligament.” Journal of Biomechanics 35 (10): 1411–15.

Wheeldon, John A., Frank A. Pintar, Stephanie Knowles, and Narayan Yoganandan. 2006. “Experimental Flexion/extension Data Corridors for Validation of Finite Element Models of the Young, Normal Cervical Spine.” Journal of Biomechanics 39 (2): 375–80.